A Quantitative Comparison of Synthetic Mammograms with Images from Conventional Mammography

Ellinor Frost

2019

Master's Thesis

in

Biomedical Engineering

Supervisors

Dr. Magnus Dustler and Prof. Hanna Isaksson

Department of Biomedical Engineering

LUND UNIVERSITY

LTH

FACULTY OF ENGINEERING

Acknowledgements

I want to thank my supervisors Magnus Dustler and Hanna Isaksson. Thank you for the help during the course of the project. Thank you Magnus, for your everyday support and for sharing your valuable knowledge. Thank you Hanna, for giving me tricky questions that made me to think ‘how’ and ‘why’.

A special thanks to Daniel Förnvik for helping me with LIBRA for density analysis, and to understand the results of my data. I am very thankful that you gave me some of your time and pedagogically explained how to use SPSS for analyses and what methods that are preferred to use and why.

Thank you LUCI, for giving me the opportunity to be a part of you. Thanks for providing materials to my project. I am very grateful for receiving the insight in how research is proceeded with article writing until publishing and funding applications. Thank you for the fun days in Brösarp and thanks for the important work you are doing.

To Siemens Healthineers, Forchheim, Germany, thank you for providing the reconstruction algorithms and for processing synthetic mammograms to my project. Thanks for hosting the nice visit and for the interesting demonstrations.

Alejandro Rodriguez-Ruiz, Radboud University Medical Center, Nijmegen, the Netherlands, thank you for helping me processing synthetic mammograms in Transpara.

Thank you gympagruppen for the 7-minutes daily movements and for the fun & laughter.

To the breakfast crew, thank you for a nice ending every week with a tasty Friday breakfast.

Thanks to my friends for your support and the good times we have had.

My warmest gratitude would I like to give to my family for always being there for me and supporting me in all decisions I make. Thanks for bringing me to where I am today!

Ellinor Frost
Dalby, 2019-03-28

Abstract

Breast cancer is the most common cancer among women in Sweden. To be able to treat the disease it is important that it is detected at an early stage. In Sweden, women between 40 and 74 years are regularly offered screening with mammography to detect abnormalities in their breasts. The mammograms give the radiologist a good image of the breasts' appearances, but it is difficult to detect structures that are covered by overlaying breast tissue, which are thus not seen in the image. To visualize structures hidden within the tissue and to see structures at different depths in the breast, breast tomosynthesis can be used. Breast tomosynthesis gives a three-dimensional image of the breast. In order to obtain the three-dimensional image, the breast is scanned in an angle of for example 50° and 25 projections of the breast are acquired. This can be reconstructed into a 3D image stack of the breast. To give an overview of what is shown in the corresponding tomosynthesis stack, the data can be reconstructed into a single synthetic mammogram. In this project, a quantitative comparison has been done between synthetic mammograms and conventional mammograms to investigate similarities and differences. The ultimate goal was to examine if it could be possible to use synthetic mammograms to compare to prior synthetic mammograms in order to track changes in the breast over time, when screening for breast cancer, just as conventional mammograms are used today. If that would be possible, the synthetic mammograms can provide a good overview of the breast, additionally the image stack acquired from breast tomosynthesis would give the radiologist the possibility to examine the breast in detail. The results showed that the synthetic mammograms were similar to conventional mammograms in one out of three aspects, the breast area density. Another comparison of the three was to use Transpara, an AI software, to examine the mammograms. This indicated similarities but there is still not enough evidence to draw conclusions. The last method of the three indicated significant differences in the frequency content, thus different structures were visible in the two types of mammograms. To conclude, synthetic mammograms and conventional mammograms are quite similar, but there are still improvements to be done before being able to state that they are equivalent.

Populärvetenskaplig sammanfattning

Bröstcancer är den vanligaste typen av cancer hos kvinnor i Sverige. Ca 7000 kvinnor i Sverige drabbas av bröstcancer varje år och 1400 av dem dör. I Sverige erbjuds kvinnor mellan 40 och 74 år screening för att upptäcka bröstcancer i ett tidigt stadie. Screening görs med mammografi och ger en två-dimensionell (2D) röntgenbild. Det kan dock vara svårt att se förändringar i bröstet på en 2D bild då avvikande strukturer i bröstet kan täckas av annan bröstvävnad och förbli oupptäckta. För att synliggöra eventuellt gömda strukturer kan brösttomosyntes användas. Vid brösttomosyntes tas till exempel 25 snittbilder av bröstet som tillsammans har ett vinkelomfång på 50°, dessa bilder ger tillsammans en så kallad ”pseudo-tre dimensionell (3D)”-volym av bröstet. Bilderna kan därefter rekonstrueras till en så kallad syntetisk mammografibild som är i 2D.

Syftet med projektet var att genomföra en kvantitativ jämförelse mellan syntetiska bilder med bilder från vanlig mammografi för att undersöka likheter och skillnader. Detta för att senare undersöka om det går att använda syntetiska bilder vid screening för att jämföra med syntetiska bilder från tidigare screeningtillfällen och se förändringar i bröstet över tid, på samma sätt som mammografibilder används idag. Om det är möjligt erhålls både en enkel överblick av bröstet som fås med den syntetiska bilden, samtidigt som det går att undersöka bröstet snitt för snitt med brösttomosyntes.

Vid screening tas bilder i två vinklar på bröstet, en bild uppifrån och en från sidan. I det här projektet användes bilder från 69 kvinnor, där alla bilder visade bröstet från sidan. Bilderna undersöktes med tre olika metoder. Med den första metoden undersöktes det om frekvensinnehållet skilde sig mellan de syntetiska bilderna och de vanliga mammografibilderna. Den andra metoden som användes var att med hjälp av mjukvaran LIBRA bestämma arean tät bröstvävnad i förhållande till det totala bröstets area på bilderna. Den tredje metoden som användes var att använda mjukvaran Transpara. Transpara använder artificiell intelligens och ger bilderna ett Transpara score på 1-10 beroende på sannolikheten för cancer på bilderna där 10 innebär att något som liknar cancer har upptäckts på bilden.

Resultatet av projektet visade att mammografibilder och syntetiska bilder erhöll liknande resultat gällande andelen tät bröstvävnad i bilderna. Däremot fanns det fler högfrekventa strukturer i de vanliga mammografibilderna än i de syntetiska mammografibilderna. Detta kan innebära att vävnad med stråkigheter i den vanliga mammografibilden, som kan ge indikation för cancer, inte finns med i den syntetiska bilden och därmed kan cancern förbli oupptäckt i de syntetiska bilderna. Användningen av mjukvaran Transpara kunde inte påvisa några skillnader mellan vanliga mammografibilder och syntetiska bilder. Det går inte att med säkerhet

bekräfta detta, då Transpara endast är tränat på att tolka vanliga mammografibilder och inte syntetiska bilder.

Det krävs mer utveckling och förbättring av de syntetiska bilderna för att få dem att likna vanliga mammografibilder. När de är förbättrade kan det kanske i framtiden bli standard med brösttomografi och syntetiska bilder vid screening för bröstcancer och strålningen från vanlig mammografi uteslutas.

Table of contents

Acknowledgements I
Abstract III
Populärvetenskaplig sammanfattning V
Table of contents VII
Abbreviations 1
1 Introduction 3
1.1 Background 3
1.1.1 The breast 3
1.1.2 Mammography and breast tomosynthesis 4
1.1.2.1 Mammography 4
1.1.2.2 Breast tomosynthesis 5
1.1.2.3 Synthetic 2D mammogram 5
1.2 Aim 6
2 Theory 7
2.1 Mammography, breast tomosynthesis and synthetic mammogram 7
2.2 Noise power spectrum 8
2.3 Density of the breast 9
2.4 Artificial intelligence, AI, for evaluation of mammograms 10
3 Method 13
3.1 Selection of images 13
3.2 Noise power spectrum - β − value calculations 15
3.3 Density measurements 16
3.4 Transpara score measurements 17
3.5 Analysis of the data 18
4 Results 19
4.1 Noise power spectrum - β − value calculations 19
4.2 Density measurements 22

4.3 Transpara score measurements 26
5 Discussion 29
5.1 β − value calculations 29
5.2 Density calculations 30
5.3 Transpara score 31
6 Ethical reflection 33
7 Conclusion 35
8 References 37
9 Appendices 41
9.1 Appendix 1 41
9.2 Appendix 2 47
9.3 Appendix 3 50
9.4 Appendix 4 50
9.5 Appendix 5 51
9.5.1 calc_digital_nps(l, n, px, use_window, average_stack) 51
9.5.2 cart2rad(nps_x, f_x, n, unq) 52
9.5.3 fit_nps(nps_in, f_in, n, nps_fun, P_start, f_fit, log_fit) 54
9.5.4 power_law_noise(P, varargin) 55
9.6 Appendix 6 56
9.7 Appendix 7 56
9.8 Appendix 8 – Results 57
9.8.1 β − value 57
9.8.2 Density measurements 59
9.8.3 Transpara score 61

Abbreviations

2D	two-dimensional
3D	three-dimensional
AI	Artificial Intelligence
AIP	Average Intensity Pixel
ANOVA	Analysis of Variance
AUC	Area Under the Curve
BI-RADS	Breast Imaging - Reporting and Data System
BT	Breast Tomosynthesis
CC	Cranio Caudal
CT	Computed Tomography
DICOM	Digital Imaging and Communications in Medicine
DM	Digital Mammography
LIBRA	Laboratory for Individualized Breast Radiodensity Assessment
MBTST	Malmö Breast Tomosynthesis Screening Trial
MGD	Mean Glandular Dose
MIP	Maximum Intensity Pixel
MLO	Medio-Lateral Oblique
ROC	Receiver Operating Characteristic
ROI	Region of Interest

1 Introduction

1.1 Background

Breast cancer is the most common cancer among women in the world [1]. Every year 7000 women in Sweden are diagnosed with breast cancer, and around 1400 die from the disease [2]. To be able to treat and cure the cancer, it is important to find it at an early stage. In order to find it at an early stage before any symptoms are shown, breast cancer screening with mammography is used. In Sweden women are offered regular screening [1, 3, 4]. The screening age and intervals may be different depending on where in Sweden women live, the intervals below are those used in Region Skåne. When women are 40-54 years and 55-74 years, they are offered screening with an interval of 18 months and 24 months, respectively [5]. The reason for having different intervals is that younger women have denser breast than older women which makes it harder to detect cancer and that breast cancer in young women can grow and develop faster despite the fact that the incidence of cancer increases with age [6].

1.1.1 The breast

The breast consists of glandular tissue and adipose (fatty) tissue, but also blood vessels, ducts for transporting milk, lymphatic vessels and lymph nodes. The breast also consists of connective tissue and ligaments that give the breast its shape. The glandular tissue is divided into 15-20 lobes and the lobes consist of smaller structures called lobules. The main task for the lobules is to produce milk when women are breastfeeding [7].

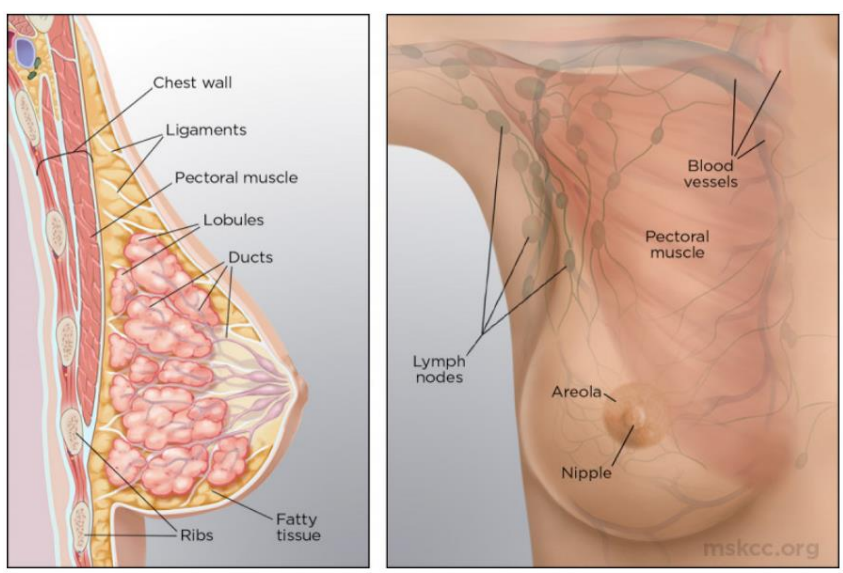

Figure 1.1: The female breast. (A screenshot from Memorial Sloan Kettering Cancer Center, 2019 [retrieved 2019 11 10]; Available from: https://www.mskcc.org/cancer-care/types/breast/anatomy-breast.)

1.1.2 Mammography and breast tomosynthesis

1.1.2.1 Mammography

Digital mammography (DM), now usually simply called mammography since the phasing-out of analogue systems, is the main technology used for breast cancer imaging. The first time X-rays were used to detect breast cancer in-vivo was at the end of the 19th century, but it was often too late to be treated [8]. The German surgeon Albert Salomon is known as the founder of mammography. In 1913 he presented how he had used X-rays on mastectomy specimens, and how it could show the distribution of cancer within the specimens [8, 9].

In 1930 Staffon L. Warren presented a stereoscopic in-vivo technique for mammography on patients undergoing surgery. In 1931 Walter Vogel presented how benign breast lesions and carcinoma could be differentiated from each other on mammograms.

Developments, discoveries and studies were made. Jacob Gershon-Cohen showed in the 1950s the correlation of lesions on roentgenograms with specimens. He also showed the importance of compressing the breast during X-ray exposure in order to receive good contrast in the image and an evenly spread radiation field [9].

The Uruguayan radiologist Raul Leborgne realised the importance of compressing the breast to mammograms with good quality, and also to visualize and differentiate different microcalcifications in breast cancer [9].

In 1960 the radiologist Robert L. Egan presented a mammographic technique that became widespread and increased the interest in mammography. This technique was reproducible and obtained high-quality mammograms in a way that had not been possible before. It could also be used for breast cancer screening [9, 10].

In Sweden in 1976 a study in Malmö was started by the radiologist and pioneer Ingvar Andersson. The purpose of the study was to investigate if regular screening for breast cancer with mammography could be a useful method. This study was the second largest study in the world. It provided the basis for regular breast cancer screening in Sweden [11].

An article published in 2016 was based on trials of breast cancer screening with mammography in Malmö, Stockholm and Göteborg. The article evaluated whether screening could reduce the risk of mortality because of breast cancer. The article included women who had their first screening in 1976 between the ages of 40-74 years and the last screening in 1986. It was shown that the risk of mortality was relatively decreased with 15% due to screening [12].

1.1.2.2 Breast tomosynthesis

Another technique for imaging the breast is with breast tomosynthesis (BT). BT is based on tomosynthesis which is in turn based on standard tomography that had its birth in the beginning of the 20th century and was developed by physicians and engineers. They combined the moveable X-ray tube and detector as well as the idea of acquiring images at different angles [13].

A research group at Johns Hopkins University, USA, was the first to use the word tomosynthesis. They had constructed a machine that could image the skull of a chimpanzee in the late 1960s. In the 1970s and 1980s better algorithms, for example deblurring for tomosynthesis was developed. Breast tomosynthesis development started in the late 1990s at the breast imaging group at the Massachusetts General Hospital, USA [13].

A study, recently done in Malmö called Malmö Breast Tomosynthesis Screening Trial (MBTST) lasted for five years (2010-2015) and included approximately 15000 women. The women had undergone two view mammography as part of their regular screening examination, that is in the medio-lateral oblique (MLO) and cranio-caudal (CC) view and one view BT in the MLO view. Results indicated more cancers were detected with BT than with conventional mammography, namely 8.7 cancers and 6.5 cancers per 1000 women screened, respectively [14].

1.1.2.3 Synthetic 2D mammogram

Today, conventional mammograms are often used together with BT. But for this the woman has to be exposed to X-rays twice, once for the one view mammography and once for the one view BT.

The MBTST showed that more cancers could be detected with BT than with conventional mammography. In the study the women had to be exposed to X-rays twice, once for the conventional mammography examination, to acquire 2D images, and once for the BT. With 2D-images of the breast, the radiologist can achieve a good overview of the breast and can easily track changes in the breast over time when comparing with prior mammograms acquired from earlier screenings.

To only use BT without any form of 2D mammograms for screening examinations, has in some studies been shown to make it hard to correctly classify clusters of microcalcifications. Because the microcalcification cluster may appear as one microcalcification on each slice, it may not be obvious that there is a cluster of calcifications, making it harder to detect [15]. BT stacks are also difficult to compare with prior screening mammograms in order to detect changes in breast composition. That is the main reason why synthetic 2D mammograms are advantageous as they will be easier and quicker to compare with prior mammograms. The synthetic 2D mammograms are synthesized from the image stacks obtained from BT.

The reconstruction algorithm, Insight2D, used in this project was developed by Siemens Healthcare in Forchheim, Germany. At the moment an improved version of the algorithm is under development. The two different types of synthetic mammograms are in this report referred to as old Insight2D and new Insight2D.

Depending on what algorithm is used for creating the synthetic 2D mammogram from tomosynthesis projections, the synthetic 2D mammogram and the mammogram acquired from DM will be more or less similar. To quantify how similar or dissimilar they appear was the purpose of this project.

1.2 Aim

The aim of the project was to make quantitative comparisons of synthetic 2D mammograms and mammograms from conventional mammography, to lay the foundation for future work to determine if synthetic 2D mammograms can be used for tracking changes in the breast over time and compare with priors, in the same way conventional mammograms are used today.

2 Theory

2.1 Mammography, breast tomosynthesis and synthetic mammogram

Breast cancer screening with mammography is used to detect cancer at an early stage. At an examination, two images of each breast are acquired, in the MLO view and in the CC view as seen in Figure 2.1. The two views complement each other; the MLO view provides a good visualization of the inner part of the breast and the pectoralis muscle, while the CC view effectively visualizes the central part of the breast [1].

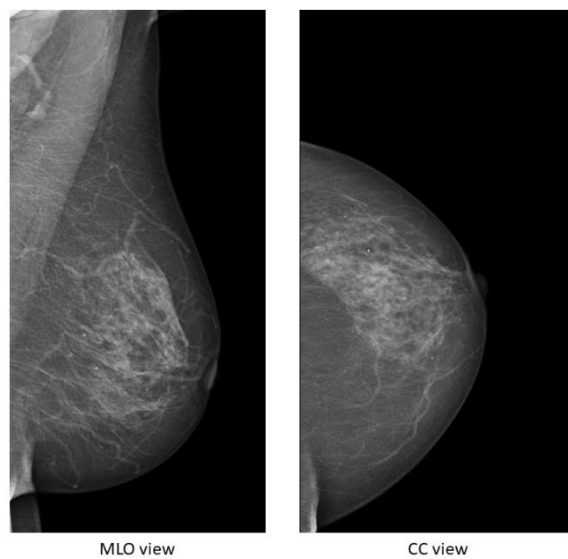

Figure 2.1: The two most common views used at mammography; medio-lateral oblique and cranio caudal. (A screenshot from Transpara.)

Breast tomosynthesis is a method that acquire images of the breast in for example 25 projections in an angle of 50° over the breast. The 25 projections acquired are reconstructed to provide a pseudo-3D volume of the breast, which gives the possibility for the radiologist to examine individual slices of the breast [13]. BT can be done in both CC and MLO views, but in this project only the MLO view has been used [13, 14].

When imaging the breast, it has to be compressed to get a good quality of the mammogram acquired, but also to reduce scattered radiation, reduce the radiation dose and to spread apart structures in the breast as a way to reduce overlaying breast tissue. The compression force in the MLO view can roughly be reduced by 40% when BT is being used instead of DM [14, 16]. The reason of a reduction in the compression force in BT is that the breast is imaged in several projections, thus the breast tissues do not have to be spread apart to the same extent as in DM. The mean glandular dose

(MGD) for a two-view, CC and MLO, DM has been reported as 2.7 mGy while for a BT in the MLO view it is 2.3 mGy [1, 13, 14, 17].

A synthetic mammogram is a 2D-image which is the result of "slabbing", that is adding the reconstructed slices of a BT-volume into a single 2D image. This is usually done either as an average intensity pixel (AIP) or maximum intensity pixel (MIP) slab. AIP means that each pixel in the image is equal to the average of the voxels projected into it, and MIP means that each pixel is equal to the maximum value of the voxels. AIP tends to hide important structures, while MIP is often excessively noisy. The Insight2D algorithm uses a blend of these two methods together with iterative image filters to produce an image. The new Insight2D is designed to create an image which looks similar to an unprocessed mammogram, which is the raw output from the X-ray detector. This allows the use of the same image filters and image processing normally employed in the mammography system to for example optimize the gray scale and equalize the contrast [18].

2.2 Noise power spectrum

A mammogram consists of layered structures of a wide range of sizes. Like in other images, the smaller the structure, the higher its spatial frequency, and vice versa, with single-pixel structures having the highest possible frequency [19].

A noise power spectrum shows the distribution and amplitudes of the spectral frequencies in the image. Assuming a perfect detector, it consists of two parts, the anatomical noise and the quantum noise [20]. Anatomical noise is the signal from, in this case the breast tissue, both normal breast tissue and abnormalities in the tissue. That means, anatomical noise can hide abnormalities that are of interest [21]. Quantum noise, or statistical noise, occurs when acquiring the image. Quantum noise may include detector noise which is caused by a non-ideal detector, in other words an ideal detector has a 100% effectiveness. Quantum noise depends on how the photons are distributed in the X-ray beam and absorbed in the tissue. To get a good image, photons need to be equally distributed in the beam. When acquiring the image, photons are never perfectly evenly distributed and that is what gives rise to the quantum noise [22]. The field becomes more even the more the breast is exposed, and the statistical noise will be lower.

The expression for the noise power spectrum, NPS(f), can be written

$$NPS(f) = NPS_q(f) + NPS_a(f) \quad (1)$$

where $NPS_q(f)$ and $NPS_a(f)$ are the quantum noise power spectrum and anatomical noise power spectrum, respectively. At low frequencies the noise power spectrum is dominated by the anatomical noise, while at high frequencies quantum noise

contributes more to the noise power spectrum than the anatomical noise. The anatomical noise power spectrum follows a power-law relation

$$NPS_a(f) = \alpha f^{-\beta} \quad (2)$$

where f is the spatial frequency, α is a scaling factor and the exponent, β controls how fast the curve increases or decreases. Studies indicate that a mammogram with a small β-value have less fibroglandular tissue in the breast, which improves detectability of abnormalities in the image[23].

Earlier studies have shown that the β-value differs depending on what modality is used. The β-value on a breast computed tomography (CT) image and a mammogram have the following relation [20].

$$\beta_{CT} = \beta_{\,conventional\,mammogram} - 1 \quad (3)$$

In conventional mammograms the β-values are between 1,5 to 3,5 [24]. A high β-value means that high spatial frequencies are dampened, and high spatial frequencies correspond to small and detailed structures in the image. That means an image with a high β-value has less detailed structures than an image with a lower β-value. Low spatial frequencies represent smooth shapes of the image [25, 26].

2.3 Density of the breast

Women with dense breasts (an increased portion of glandular and fibrous tissue compared to adipose tissue) have a higher risk of developing breast cancer than women with less dense breast [27]. At the same time, it is also more difficult to detect abnormalities in dense breasts since it may be hard to palpate abnormalities, and also hard to detect them in mammography screening since they may be covered by overlaying tissue. Besides, dense tissue and both benign and malignant tumors have similar attenuation of X-rays [28, 29]. Mammographic density classification of the breast is today visually done by the radiologist when examining the mammogram. The density of the mammogram can for example be graded according to the Breast Imaging-Reporting and Data System (BI-RADS) density estimation [29]. The BI-RADS's grading scale is a – d, the different grades in the scale represent different fibroglandular tissue content and distribution in the breast, and hence the breast density. The different grades are: a: the breast almost only consists of adipose tissue, b: mostly adipose tissue but there are scattered areas with fibroglandular tissue, c: heterogeneously dense breasts, and d: extremely dense breast [30].

The density of the breast can as mentioned be subjectively visually rated, but it can also be quantitatively derived. There are two different kinds of measurements that refer to the amount of dense tissue in the breast. One is volumetric measurement which is a relation between the volume of the dense tissue in the breast compared to the total

volume of the breast. The breast volume can be measured in many ways with different methods, for example, with imaging or with biostereometrics methods [31, 32]. The most commonly used method is to determine the density based on relative attenuation properties of breast tissue. According to this method there are two types of tissues in the breast, dense fibroglandular tissue and adipose tissue. From the image it is estimated how much a certain thickness of adipose tissue attenuates the radiation. With that in mind the relative densities of each pixel are estimated depending on the thickness of the tissue and the detected relative attenuation [33].

Another way to measure the density is to take the breast area into consideration, instead of the volume, similar to an assessment done by a radiologist. In this project the breast density was measured with the software Laboratory for Individualized Breast Radiodensity Assessment version 1.0.5-beta1, LIBRA, which measures the area density of the breast. LIBRA processes the image while first marking the boundary of the breast and the pectoralis muscle. Thereafter, it uses an algorithm that segments the breast into regions and group them together depending on their grey-scale levels, thus the same X-ray attenuation. The area of the regions which are defined to be dense tissue is then added together to a total dense area of that specific breast. The breast density is calculated by

$$breast\ density = \frac{dense\ breast\ area}{total\ breast\ area} * 100 \quad (2)$$

where the areas are in square centimeters (cm^2) and the breast density in percentage (%) [34-36].

2.4 Artificial intelligence, AI, for evaluation of mammograms

The mammograms obtained during examinations are preferably examined by two independent breast radiologists in order to find abnormalities, and to reduce recalls of false-positive cases. This is a time and cost consuming method; therefore, alternatives would be welcome. To make the examinations of mammograms more efficient AI methods could be used. An AI system developed by ScreenPoint Medical BV, Nijmegen, the Netherlands, called Transpara 1.4.0 (hereinafter called Transpara) has been used in this project. Transpara has been trained and taught using deep learning methods to differentiate cancer in the form of calcifications and soft tissue lesions on mammograms. In order to teach the system how to differentiate structures, it was trained on 45000 mammograms that were classified using a number of different traditional image classification methods developed from earlier computer-assisted detection (CAD) systems for mammography. Together with information of the diagnosis of each image, a deep-learning convolutional neural network was used to train the system to find and rate lesions according to their suspiciousness [37].

Transpara scores suspicious regions on mammograms by giving them a cancer likelihood score from 1-100. It interacts with radiologists by giving them the local score, if the score is >15, of a selected area [38, 39]. Based on the type of findings and level of suspiciousness on the mammograms, Transpara gives one overall score for that specific examination. The Transpara score is a score from 1-10, where 10 represents something that has the highest risk of being malignant while 1 represents that nothing suspicious can be proved. In a typical screening population, the programme has been calibrated to put 10% of cases in each category and >80% of cancers in group 10 [38, 40].

3 Method

The following chapter describes the method used. It starts to describe how the selection of images was done and follows with three parts used for the mammogram analysis. It ends with the statistical analysis of the received data. A visual overview can be seen in Figure 3.1.

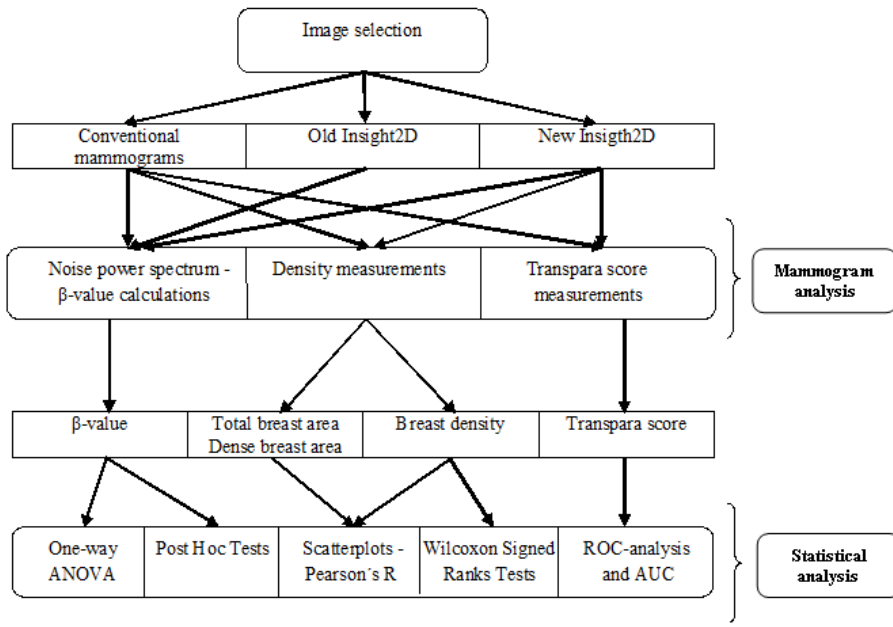

Figure 3.1: A schematic overview of the different steps in the method.

3.1 Selection of images

The images from DM used in this project were selected depending on the Transpara score they had received from an evaluation not connected to this study, and also depending on the findings on the DM images, that is the type of case-group each of the mammograms is connected to (left column in Table 3.1) [14, 41]. As mentioned before Transpara scores the mammograms depending on their probability to contain tumors. The higher score the higher probability there is to find anything malignant in the mammograms.

In total 69 cases, that is 69 DM images, were selected from four different groups. The division of the groups depended on what each individual case at the end turned out to be. The groups contained false-negative cases, false-positive cases, true-negative cases and true-positive cases.

- False-negative case: the result pointed to no malignancy, but the case proved to be cancer. This type of cancer is called interval cancer and is often detected by the woman between two consecutive screening examinations.
- False-positive case: the result pointed to cancer, but it was not [31]. When the radiologist finds something suspect in the image, the woman is recalled for further examinations. But the findings from the further examinations do not show any malignancy.
- True-negative case: the result points to no cancer, and there was no cancer. No interval cancer is detected between two consecutive screening examinations.
- True-positive case: the result points to cancer, and it was cancer [32]. That is also when the woman is recalled for further examinations the finding verifies malignancy.

At the beginning, 20 cases were chosen from each group except the group containing false-positive cases where only 19 cases were chosen. In addition, the cases were chosen so ten of the 20 cases had a high Transpara score while the other ten had a low score. During the process of the project some of the cases were excluded, thus reducing the number of cases. This was because one case had only one mammogram, some cases had mammograms with artefacts while several cases had mammograms in only the CC view. However, this project only considered images in the MLO view as these were the only BT projections available. In Table 3.1, the number of cases from each group can be found, and how high and low Transpara score was defined for each group.

Table 3.1: The number of cases from the different case groups. The Transpara score refers to the image acquired from mammography.

Types of cases	**Low/high Transpara score**	**Transpara score**	**Number of cases**
False-negative	Low	< 8	7
	High	> 9	7
False-positive	Low	< 3	9
	High	> 9.8	9
True-negative	Low	< 0.1	10
	High	> 9.96	10
True-positive	Low	< 6	7
	High	> 9.96	10

Every woman had undergone BT, in this case stacks with 25 images of each breast were yielded. Based on the raw data from the BT two different types of synthetic mammograms were created. In total 414 different images were analyzed, 69×2 mammograms from DM, 69×2 old Insight2D and 69×2 new Insight2D. All the different kinds of mammograms were acquired on Mammomat Inspiration Tomo (Siemens Healthcare GmbH, Erlangen, Germany).

In this project, only mammograms in the MLO-view were used, since examinations with BT had only been done in the MLO-view, and hence, there were only synthetic mammograms in the MLO-view available.

3.2 Noise power spectrum - β – value calculations

As mentioned in the theory in chapter 2.2, the noise power spectrum is a spectrum of the spatial frequencies in the image. The purpose with this analysis was to investigate if the frequency content changed between conventional mammograms and synthetic mammograms. The frequencies relevant for the investigation were those responsible for the anatomical noise, namely the structures of the breast. It was assumed, that the total noise power spectrum follows the same power-law equation (2) as the anatomical noise does. An overview of the calculations implemented can be seen in Figure 3.2. To be able to only use the frequencies responsible for the anatomical noise, the image was loaded into MATLAB R2016a (hereinafter referred to as Matlab). A script (see Appendix 1) was used that created 100 regions of interest (ROIs) with a size of 100×100 pixels randomly within the breast.

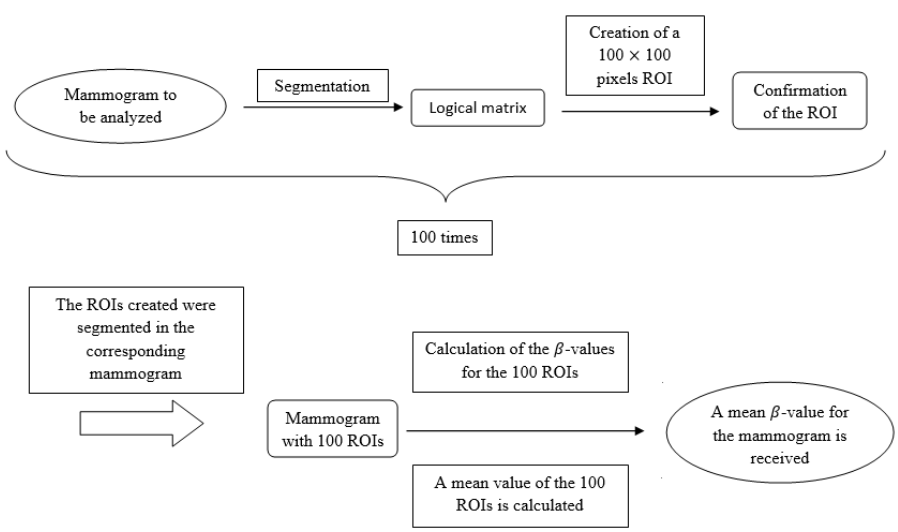

Figure 3.2: A visualization of the β-value calculations.

To make sure that the ROIs were within the breast's area on the image, the image was first converted to a logical matrix, containing only ones and zeroes, where the pixels that had a pixel value >0 became ones in the logical matrix and the rest zeros. That means that all the pixels within the breast were represented by ones in the logical matrix, and everything around the breast were zeros. Thereafter, all the coordinates of the pixel elements consisting of ones were randomly placed in a vector. For an ROI to be created, the first element from the vector was chosen, and a ROI was created with the picked element making the upper left corner of the ROI. To make sure that all the elements within the created 100×100 pixels ROI were within the breast's area, thus only had elements of ones, the sum of all matrix elements was calculated to investigate if the sum was equal to 10000. If the sum was not 10000, that meant that the current ROI was not within the breast area and a new element in the random vector had to be picked. Additionally, the sum of all the pixel elements had to be controlled. Once all the ROIs were created and all of them were within the breast in the logical matrix, the same coordinates were used to make ROIs in the corresponding breast image, from which the value of β in the noise power spectrum was calculated.

Thereafter, each ROI was processed in the script presented in Appendix 2, which calls the four scripts in Appendix 5 and calculates the β in the noise power spectrum for each ROI [42]. The scripts perform a directionally independent frequency space transform of the ROI. Thereafter, an exponential curve is fitted to the frequency spectrum and the β-value is determined, that is the exponent of the curve. A mean value of β was calculated from all the 100 ROIs in every image processed.

The script in Appendix 3 was used to load the set of images to examine, followed by the script in Appendix 4, which automatically lead the set of images through the process of making the ROIs, and thereafter, calculating and saving the β-value in the power-law equation.

The β-value was calculated on all the three types of mammograms.

3.3 Density measurements

The breast area density for the images was calculated by using the software LIBRA. Matlab was used to control LIBRA to be able to analyze the images.

To be able to analyze the synthetic mammograms the DICOM header had to be modified. The tag *ImagesInAcquisition* was removed, because it noted that there was a stack of images even if there was not. This was done in Matlab by using the script in Appendix 6.

To start the analysis, LIBRA was started and the file with images to be processed was chosen. The results obtained from LIBRA were measures on the breast densities and mammograms with breast segmentations.

Conventional mammograms and new Insight2D were analyzed in LIBRA. The old Insight2D mammograms were not analyzed, because it was shown that there was a too bright breast skin line on the mammograms. The bright skin line made it difficult for LIBRA to mark it and the pectoralis muscle, and thus, to make a correct calculation of the breast density.

3.4 Transpara score measurements

To decide the Transpara score for the different cases, the software Transpara was used. The Transpara scores for the conventional mammograms did not need to be calculated, since their scores had been measured in earlier studies and the results could be used in this project.

To be able to decide the Transpara score for the new Insight2D, the DICOM header had to be changed. Because in the header it was stated that every single image was a stack of slices acquired from breast tomosynthesis, but a synthetic image is as mentioned, only one picture and created from a stack of images. That was why the header had to be changed, so that the header information correlated with the image processed, and to make it possible for Transpara to process the image. The tags that were changed or modified were Image Type, Series Description, Acquisition Number, and Images In Acqusition, and their "values" were set to be 'DERIVED\PRIMARY\TOMO_2D\LEFT (or RIGHT)', 'T_PR L_MLO (or R_MLO) PRIME, Diagnosis', '1' and '1', respectively. These changes were done in Matlab by the script in Appendix 7. Thereafter, the new Insight2D could be analyzed in Transpara.

Once the mammograms had been processed the results could be shown in two different ways, either as an overall score namely a Transpara score of the images with the same identification number or as separate scores on all the findings on the different images. The conventional mammograms had one overall Transpara score, since all the images from the same woman had the same personal number. However, that was not the case for the synthetic mammograms, they all had different identification numbers no matter if they were from the same woman or not. That meant, that every synthetic mammogram got its own Transpara score. Therefore, the synthetic mammogram with the highest score in the set of mammograms, that is from the same woman, represented the Transpara score for that specific pair of mammograms.

The mammograms receiving a Transpara score were the conventional mammograms and the new Insight2D. The old Insight2D could not be processed in Transpara because of the time limitation of this project. Since their DICOM header on the mammograms was not accepted, and it was difficult to solve the issue.

3.5 Analysis of the data

The next step in the analysis process of the different kinds of mammograms was to evaluate the results received from the different methods, in other words the calculations of the β-value, the area density measurements and Transpara score.

The data was statistically analyzed with SPSS (IBM SPSS Statistics). To receive inspiration and suggestions about what different statistical methods were available to use for evaluating the data, different resources were used. SPSS's own menu with statistical methods, in combination with article [43] and personal communication with Daniel Förnvik gave a good combination of suggestions on methods of how to analyze the obtained data.

Different statistical methods were used that depended on the statistically distribution of the results, all results were visualized in histograms. If the result was normal distributed, parametric methods such as one-way analysis of variance (ANOVA) or Student's t-test could be used, with additional Post Hoc Tests. That was the case for the β-value results. For non-normally distributed data, non-parametric methods were used for example Wilcoxon signed rank test and in addition scatterplots for calculation of Pearson's R. The results from the density measurement was analyzed with non-parametric methods. An receiver operating characteristics (ROC) analysis was an appropriate method for the Transpara score analysis. Since the Transpara score gives a score depending on the likeliness for cancer, the scores could be evaluated in an ROC analysis. An ROC curve is usually used to evaluate the performance of the modality used and if it is 'true' or 'false', but in this case it was only used to compare the area under the curve (AUC) not to evaluate Transpara. The closer the AUC value the more similar features and structures were the mammograms assumed to have. But this analysis could be used since there were 31 cases with cancer (true) and 38 were normal (false) that is healthy cases. Transpara is not trained on synthetic mammograms that was why the ROC analysis was not used to evaluate Transpara.

4 Results

Figure 4.1 shows the left breast from the same woman. The figure shows all three types of mammograms used in this project, that is conventional mammograms, old Insight2D and new Insigh2D.

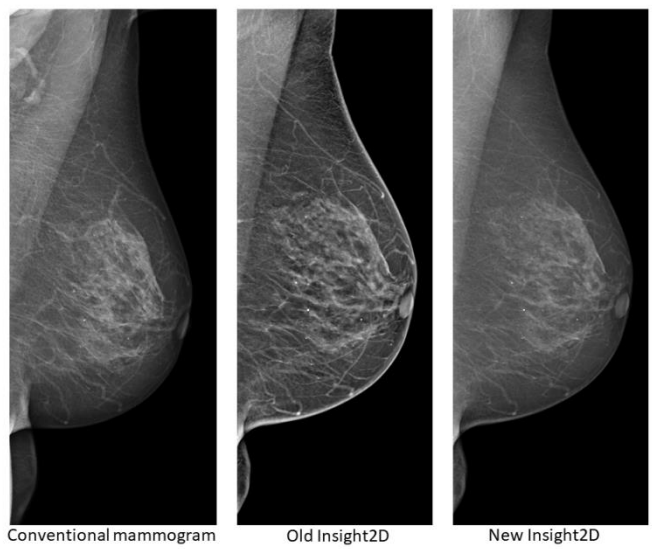

Figure 4.1: The different types of mammograms used in the project. (Mammograms saved from ImageJ.)

All data received were visualized in histograms, Appendix 9.8.

4.1 Noise power spectrum - β – value calculations

The different results received from the β-value calculations were visualized in histograms, Appendix 9.8.1. It turned out that all of them except the one for old Insight2D for the right breast were normally distributed. Since only one histogram deviated from the others and the number of cases were >50 it was acceptable to evaluate the data with parametric methods, based om the mean value of the populations. The Tables 4.1, 4.2, and 4.3 show properties of the different types of mammograms. The β-value for conventional mammograms were 1.73 ± 0.12 and 1.72 ± 0.11, for left and right breasts, respectively. For the different types of synthetic mammograms, the β-values were 3.60 ± 0.16 and 3.61 ± 0.15 for the old Insight2D left and right breasts, respectively. And for the new Insight2D 3.69 ± 0.07 and 3.69 ± 0.07 for left and right breast, respectively. A graphical illustration of this can also be found in Figure 9.4.

Two one-way ANOVA analyses were done. One analysis comparing the β-values of mammograms of the left breasts and the second analysis comparing mammograms of the right breasts.

Table 4.1: β-values for conventional mammograms.

	Conventional mammograms	
	Left	**Right**
Mean	1.73	1.72
Std. Deviation	0.12	0.11
Minimum	1.46	1.40
Maximum	1.96	2.00

Table 4.2: β-values for old Insight2D.

	Old Insight2D	
	Left	**Right**
Mean	3.60	3.61
Std. Deviation	0.16	0.15
Minimum	3.19	3.21
Maximum	3.92	3.87

Table 4.3: β-values for new Insight2D.

	New Insight2D	
	Left	**Right**
Mean	3.69	3.69
Std. Deviation	0.07	0.07
Minimum	3.53	3.53
Maximum	3.83	3.82

The ANOVA analyses showed significant differences ($P < 0.001$) between the different mammogram types. To investigate if the mean values of all the three groups differed a Post hoc test was done with a 95% confidence interval. The results can be seen in Table 4.4 and 4.5. The mean values were significantly different, which could be assumed at least between conventional mammograms and the both types of synthetic mammograms. There was also a significant difference between the two types of synthetic mammograms which was less obvious, as can be seen from the confidence intervals.

Table 4.4: Post Hoc Tests of β-values for mammograms showing the left breast.

Left breast				**95% Confidence Interval**	
(I)	**(J)**	**Mean Difference (I-J)**	**P**	**Lower Bound**	**Upper Bound**
Conventional mammograms	**Old Insight2D**	-1.88	P < 0.001	-1.92	-1.83
	New Insight2D	-1.96	P < 0.001	-2.01	-1.91
Old Insight2D	**Conventional mammograms**	1.88	P < 0.001	1.83	1.93
	New Insight2D	-0.09	P < 0.001	-0.14	-0.04
New Insight2D	**Conventional mammograms**	1.96	P < 0.001	1.91	2.01
	Old Insight2D	0.09	P < 0.001	0.04	0.14

Table 4.5: Post Hoc Tests of β-values for mammograms showing the right breast.

Right breast				**95% Confidence Interval**	
(I)	**(J)**	**Mean Difference (I-J)**	**P**	**Lower Bound**	**Upper Bound**
Conventional mammograms	**Old Insight2D**	-1.89	P < 0.001	-1.94	-1.84
	New Insight2D	-1.97	P < 0.001	-2.02	-1.93
Old Insight2D	**Conventional mammograms**	1.89	P < 0.001	1.84	1.94
	New Insight2D	-0.08	P < 0.001	-0.13	-0.04
New Insight2D	**Conventional mammograms**	1.97	P < 0.001	1.93	2.02
	Old Insight2D	0.08	P < 0.001	0.04	0.13

4.2 Density measurements

Conventional mammograms and new Insight2D were analyzed with LIBRA, to decide the percentage area of dense tissue. Images of what LIBRA decided to be dense tissue can be seen in Figure 4.2. As seen in the figure, LIBRA marks the contour of the breast and the pectoralis muscle before calculating the breast density. The results can be seen in Table 4.6 and 4.7. To note; the breast density in the tables do not agree with the ratio between the dense area and the total area seen in the same tables.

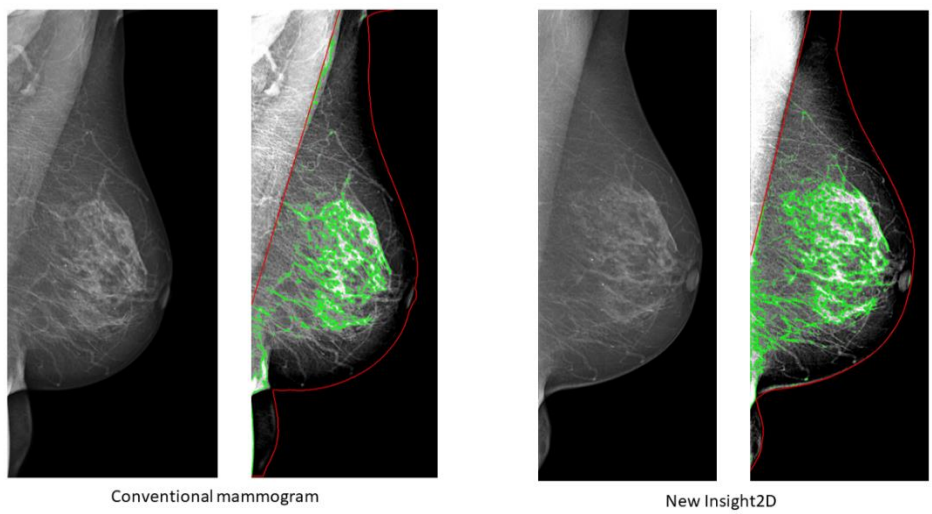

Figure 4.2: Dense breast areas within green markings and the breast contour marked in red determined by LIBRA. The left mammogram of each pair shows the corresponding mammogram without any markings. (Mammograms saved from LIBRA.)

The results obtained from all the different cases were also used for making histograms. All the different histograms, Appendix 9.8.2 (Figure 9.5-9.7), showed lop-sided distributions of the total area, the dense area and the breast density. Thus, a non-parametric statistical analysis was used. Three scatterplots comparing the different measurements, the total area, the dense area and the breast density, were created, Figure 4.3 and 4.4, and Pearson's correlation coefficient, R, was decided. The R-values were 0.87 for the total breast area for both left and right breast and 0.85 for the dense breast area for both breasts. The R-values for the breast density were similar between the left and right mammograms (R = 0.89 and 0.88). R-values (Table 4.8) showed strong correlations and no significant difference between the image types.

The scatterplots and Pearson's coefficient were used to pairwise compare the mammograms. Additionally, the Wilcoxon signed rank test was used to evaluate if the two types of mammograms had similar breast density. Table 4.9 shows, that conventional mammograms showed slightly higher breast density than the new Insight2D. The result is not significant (P = 0.26 left breast and 0.30 right breast).

Table 4.6: Properties of conventional mammograms showing left and right breast, respectively.

	Conventional mammograms					
	Left breast			**Right breast**		
	Total breast area (cm^2)	***Dense breast area (cm^2)***	***Breast density (%)***	***Total breast area (cm^2)***	***Dense breast area (cm^2)***	***Breast density (%)***
Mean	166.4	40.0	25.8	165.2	40.7	26.7
Median	157.4	34.8	22.3	157.3	34.3	23.3
Minimum	77.6	12.0	5.1	80.0	15.9	7.7
Maximum	324.9	117.7	71.7	372.3	91.2	69.5
Interquartile Range	71.1	21.9	20.1	73.9	32.9	23.1

Table 4.7: Properties of new Insight2D showing left and right breast, respectively.

	New Insight2D					
	Left breast			**Right breast**		
	Total breast area (cm^2)	***Dense breast area (cm^2)***	***Breast density (%)***	***Total breast area (cm^2)***	***Dense breast area (cm^2)***	***Breast density (%)***
Mean	151.9	34.8	24.8	148.6	36.7	26.5
Median	146.0	28.4	21.0	143.0	32.3	22.0
Minimum	77.9	10.8	6.1	74.4	8.3	3.4
Maximum	297.4	104.5	71.3	298.6	99.1	69.4
Interquartile Range	58.2	21.1	19.3	49.4	25.9	21.6

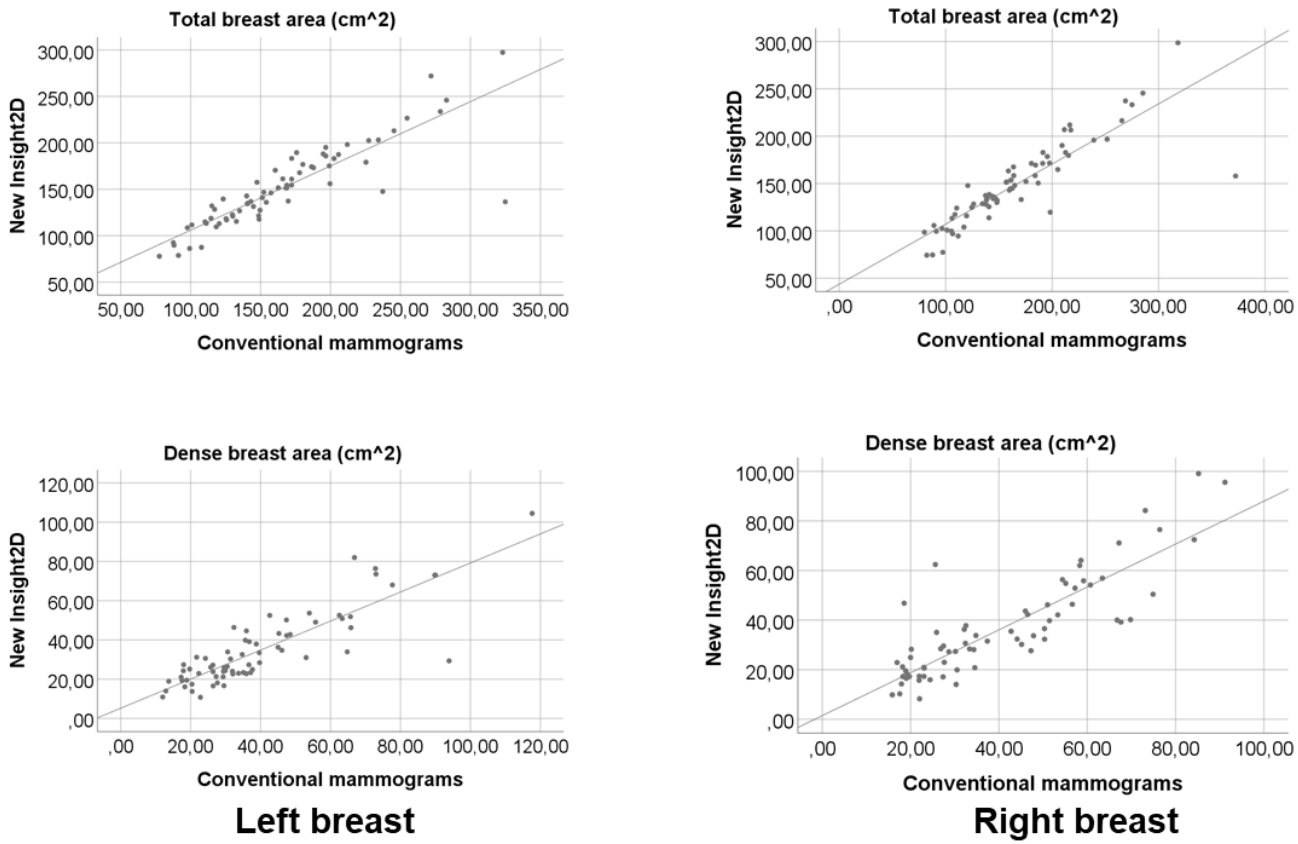

Figure 4.3: Scatterplots of conventional mammograms and new Insight2D of left and right breast, respectively. They show the total breast area and the dense breast area.

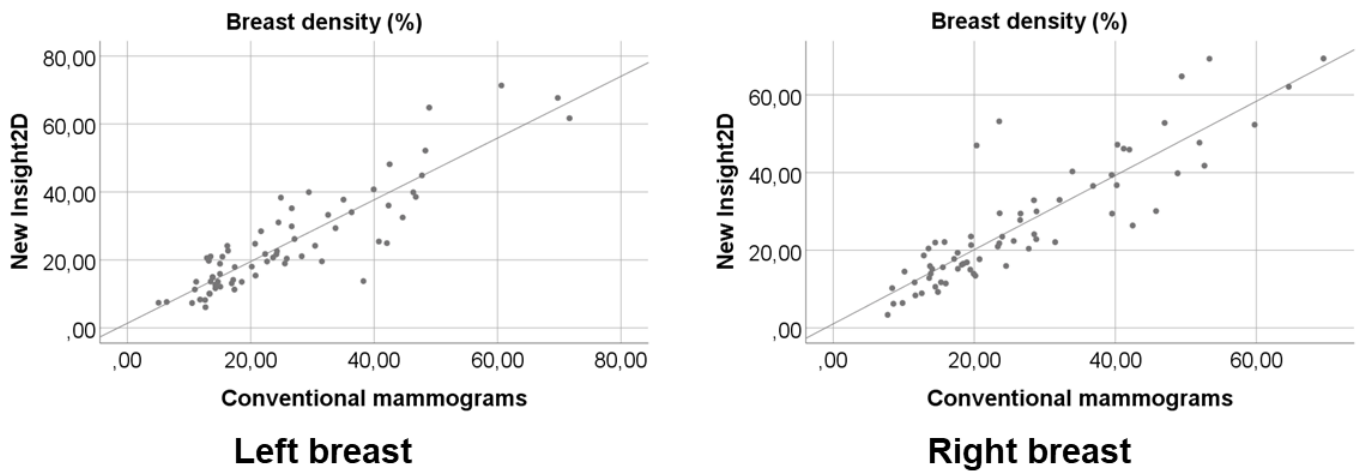

Figure 4.4: Scatterplots of conventional mammograms and new Insight2D showing left and right breast, respectively. The scatterplots show the breast density.

Table 4.8: Pearson's correlation coefficient for the scatterplots above (Figure 4.3-4.4).

Data sets to be compared		R^2	R
Total breast area	**Left breast**	0.755	0.87
	Right breast	0.751	0.87
Dense breast area	**Left breast**	0.728	0.85
	Right breast	0.726	0.85
Breast density	**Left breast**	0.790	0.89
	Right breast	0.773	0.88

Table 4.9: Wilcoxon Signed Ranks Test based on the breast densities.

			N	Mean Rank	P
Density(Conventional mammograms) – Density(New Insight2D)	**Left breast**	***Negative ranks***	30[a]	33.90 %	0.26
		Positive ranks	39[b]	35.85 %	
	Right breast	***Negative ranks***	30[c]	34.37 %	0.30
		Positive ranks	39[d]	35.49 %	
a. Density(Conventional mammograms) < Density(New Insight2D)					Left breast
b. Density(Conventional mammograms) > Density(New Insight2D)					Left breast
c. Density(Conventional mammograms) < Density(New Insight2D)					Right breast
d. Density(Conventional mammograms) > Density(New Insight2D)					Right breast

4.3 Transpara score measurements

Conventional mammograms and the new Insight2D were evaluated by Transpara, Table 4.10. Histograms to visualize the Transpara score for the mammograms can be found in Appendix 9.8.3. There were in total 69 pairs of cases, where 31 cases showed breast cancer and 38 no cancer.

Table 4.80: Transpara score on the mammograms.

	Conventional mammograms	**New Insight2D**
Median	10	9
Minimum	1	2
Maximum	10	10
Interquartile Range	7	3

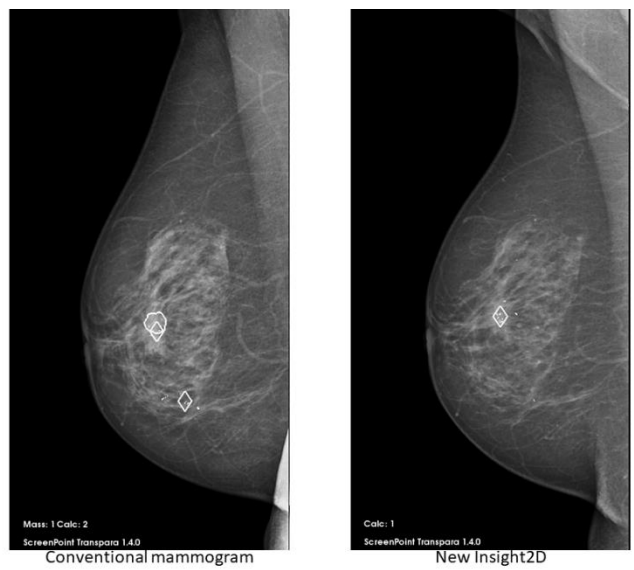

Figure 4.5:Mammograms with markings of suspicious regions determined by Transpara. (A screenshot from Transpara.)

The ROC curves can be seen in Appendix 9.8.3.

The following Table 4.11 shows results from the ROC analysis. The AUC were 0.62 for the conventional mammograms and 0.54 for new Insight2D. While the lower and upper boundaries were 0.49 and 0.75 for the conventional mammograms and 0.40 and 0.68 for the new Insight2D. Since the ranges for the boundaries were overlapping, they imply that there were no differences in the Transpara scores between the different mammograms.

Table 4.11: ROC and AUC comparison on two types of mammograms. The purpose was to evaluate if the AUC values were similar, not to evaluate Transpara.

	Receiver operating characteristics (ROC)		**Area under the curve (AUC)**		
	N			**Asymptotic 95% confidence interval**	
	Positive cases	**Negative cases**	**Area**	**Lower bound**	**Upper bound**
Conventional mammograms	31	38	0.62	0.49	0.75
New Insight2D	31	38	0.54	0.40	0.68

5 Discussion

The aim of this project was to compare conventional mammograms and synthetic mammograms. The methods used were to compare the frequency content in the mammograms, the area breast density and the Transpara score. The result showed that the mammograms had significant different frequency content. The breast densities were well correlated between conventional mammograms and new Insight2D but for the old Insight2D there was a difference. This means, improvements have been done in the reconstruction's algorithm for creating synthetic mammograms. The Transpara score were also similar when comparing the AUC-values, but more cases for that method are needed. The different methods and results will be discussed under the following subchapters.

5.1 β – value calculations

When the logical matrix was created, while preparing for making the ROIs, pixels with a value >0 became ones, and pixels with a value equal to 0 became zeroes. In the ideal case pixels with a value >0 should only be found within the contour of the breast and nowhere around the breast. It was unknown if pixels for example artefacts could have led to pixels outside the breast's boundaries being >0, but this is unlikely as image processing should take care of this. However, if there were pixels with a value >0 where they should not be, then those frequencies could have affected the estimated β-value. To avoid extra pixels and mammograms with artefacts or anything else, every mammogram would have to be examined. In the interest of time, no mammogram was reviewed in such a way before being used in this project. All the mammograms were from examinations and processed using standard software supplied by Siemens and were assumed to be of good quality, if not new mammograms were acquired.

When creating the ROIs, it was confirmed that the whole ROI was within the contour of breast, but it was not verified whether the different ROIs overlapped with each other or not. This simplified the writing and execution of the script, and any statistical problems caused by this should be compensated for due to the randomized center approach used and due to the large number of samples.

The estimation of the β-value was intended to determine if the different types of mammograms had the same frequency content. The β-value does not quantify the spatial distribution of frequencies. So, basically the β-exponents can be the same, but the mammograms can look completely different, they just have the same frequency content, or size distribution of structures. This is something to be aware of, as it can mean that on the conventional mammogram very important structures can be seen but may have disappeared on the synthetic mammogram, for example fine high-frequency spiculations that characterize the border of a malignant lesion. The synthetic

mammogram may instead have other structures that may be irrelevant, but they cause the β-value to be the same.

The results of the β-values were significantly different when comparing all the cases. High β-value for the synthetic mammograms indicates, according to the power-law equation, that high frequencies are being more dampened compared to low frequencies than on conventional mammograms. High frequencies are those frequencies that make up small and detailed structures. Consequently, if the high frequencies are dampened there is a risk that essential structures disappear from the mammograms which can be severe. It could be that such structures are the only indications of cancer. If the structures are lost the cancer is missed. The damping of the high frequencies can also be seen if comparing the mammograms in Figure 4.1. The synthetic mammograms have less details than the conventional mammograms. However, the effect of this on image quality is unknown. This study did not evaluate if lesion visibility was affected.

5.2 Density calculations

For the breast density calculations only conventional mammograms and the new Insight2D were used. Early in the project a few old Insight2D were processed in LIBRA, but without any success in calculating the breast densities. The densities obtained had major deviations from normal densities which were obviously a result of the marked dense areas on the mammograms. As can be seen in Figure 4.1, there is a very bright skin line contour around the breast that made it hard for LIBRA to firstly segment the breast and the pectoralis muscle, and thereafter segment the dense areas based on the marks. Thus, early on, the old Insight2D were excluded from the density calculations. Because it was evident, they were different compared to the conventional mammograms and new Insight2D.

Interesting observations that can be noted in Table 4.6 and 4.7, all areas and the densities are bigger for the conventional mammograms than for new Insight2D. This may be a result of the different compression magnitude used at the mammography versus breast tomosynthesis. For conventional mammography the breast had to be more compressed to receive a mammogram with good quality in comparison to breast tomosynthesis where force did not need to have that big magnitude to receive a good image [14]. Since the breast is not so compressed, the area of the breast is smaller for breast tomosynthesis and synthetic mammograms, than it is on conventional mammograms.

The scatterplots, Figure 4.3 and 4.4, were created to visualize the areas and densities, and for calculating Pearson's R do all have similar scatter variation. All of them have very little scatter at low values while mammograms with greater areas and densities

have a bigger distance to the straight line. The figures (4.3 and 4.4) appeared as expected. Furthermore, the Pearson's coefficient indicated on a strong correlation between every pair of mammograms.

There seems to be a systematic offset with approximately 2%-points for the different breast densities if the calculations are done with a calculator. When calculating the ratio between the dense area and the total area the results do not agree with the results in Table 4.6 and 4.7, what LIBRA calculated. One reason for the offset could be that when LIBRA calculates the total breast area it takes the whole breast into account, including the pectoralis muscle. But when it calculates the breast density it takes the ratio between the dense breast area and total breast area, but it does not include the area for pectoralis muscle in the total area, since the dense area does not include the muscle. Another suggestion for the 2%-points difference could be that LIBRA calculates the ratio between the dense area and the total area, and thereafter makes the corrections needed for the pectoralis muscle.

5.3 Transpara score

The images processed in Transpara were those required from conventional mammography and the new Insight2D. Before Transpara could process the new Insight2D, the DICOM headers had to be slightly changed since Transpara is not trained to interpret synthetic mammograms. Changing tags in the DICOM header for the new Insight2D was done with help from Alejandro Rodriguez-Ruiz, Radboud University Medical Center, Nijmegen, the Netherlands. It was more difficult to make the DICOM header for the old Insight2D to look like the DICOM headers in the conventional mammograms. That is why they were not processed in Transpara, and due to the time limitations.

Since Transpara is not trained on synthetic mammograms, the Transpara scores given to the new Insight2D should be interpreted with care. That same is true of the evaluation of the data received. The data were analyzed with ROC analysis and the AUC was calculated. It was shown that the AUC for the new Insight2D was less than for the conventional mammograms. But there were still no significant differences between the two types of mammograms since the lower and upper boundaries overlapped. The fact that the difference was not bigger than this is promising, as it means that the system used to detect and mark cancer lesions on conventional mammograms can handle synthetic images reasonably well, which in turn indicates that the difference between the two image types is relatively minor.

However, no general conclusion can be made for the Transpara score since more cases should have been used to give the statistical analysis more strength, the 69 cases used were not enough. An essential point is that Transpara has not been trained on synthetic mammograms. The Transpara scores for the conventional mammograms were

determined based on four mammograms, two in MLO view and two in CC view from the left and right breast, respectively. The new Insight2D were only available in the MLO view and Transpara used individual scores for each mammogram, because the DICOM header did not indicate that they were pairs of mammograms from 69 women. The highest score from every pair of the new Insight2D was used for the analysis, in the same way as Transpara does, but having the CC view available as well would likely have changed the result. In addition, the cases used for the project had either low or high Transpara score, so there were very few cases with scores in between. This will affect the ROC curve, but for the analysis done in this study this should have little effect.

6 Ethical reflection

No specific ethical approval was needed for this project, since the images used were from the Malmö Breast Tomosynthesis Screening Trial, MBTST [14], which has already gone through ethical review and approval. The existing ethical review also covers extra projects like this one aimed at analyzing new reconstructions' algorithms. MBTST is approved by the ethics committee at Lund University and the Radiation Safety Board at Skåne University Hospital, Malmö. Furthermore, it is registered at ClinicalTrials.gov with the NCT number: NCT01091545.

The mammograms were already acquired before the project started, so no women had to undergo any additional examination, neither mammography nor breast tomosynthesis. Thus, they were not exposed to any additional radiation.

The synthetic mammograms created from breast tomosynthesis, were only in the MLO view, and with reduced compression compared to conventional mammography. If the synthetic one-view mammograms, namely only MLO view, in combination with breast tomosynthesis can be an alternative for breast cancer screening, the radiation dose would be slightly reduced by up to 0.4 mGy MGD, since images will only be, in this case, acquired in one view, MLO, compared to today's two-view conventional mammograms, MLO and CC, even though the dose per view would be somewhat higher. If used to replace two-view conventional mammography and breast tomosynthesis with two-view synthetic mammography and breast tomosynthesis the dose saving would be equivalent to one two-view conventional mammography examination, or roughly 2 mGy MGD.

By using synthetic mammograms, the compression of the breasts could also be reduced to about half, as breast tomosynthesis requires less compression [14]. The effect of compression on synthetic mammograms has however not been evaluated. The fear of pain during breast cancer screening is one of the main reasons women point to when they decide not to attend the screening [1]. Thus, using synthetic mammograms instead of conventional mammograms can be an alternative to both reduce the radiation dose, the compression of the breast and consequently the pain during screening. If more research is done on the two different types of mammograms and it indicates that they are sufficiently similar, it could then be possible to only use synthetic mammograms, and breast tomosynthesis, during screening and compare those to priors as conventional mammograms are used today.

7 Conclusion

Conventional mammograms and synthetic mammograms performed similarly regarding the Transpara score and the breast density. However, not so much trust can be put in analysis of the new Insight2D processed in Transpara and LIBRA since neither system is intended to work on synthetic mammograms. Additionally, there were too few cases to make any statistical conclusions from the data received from Transpara.

The breast densities were well correlated, which was also found by others [35]. Every pair of mammograms of the two different image types were well correlated. It was also a good correlation when comparing the two different groups of mammograms, conventional and new Insight2D.

There was a significant difference between the synthetic mammograms and the conventional mammograms regarding the β-values. There was also a small difference between the old Insight2D and the new Insight2D. This can be a potential risk since the β-values for the synthetic mammograms were higher than for conventional mammograms. And a high β-value means high frequencies are being dampened which can lead to essential structures not being detected.

To conclude, synthetic mammograms need improvements before they can substitute conventional mammograms during screening. They seem to show less fine structure than conventional mammograms, which is proven by the β-value calculation. The Transpara score indicated similarities even though there were too few cases to base the result on. But synthetic mammograms are as good as conventional mammograms when it comes to the breast density.

8 References

1. Dustler, M., *Pressure distribution in mammography. Mechanical imaging and implications for breast compression*. 2016: Lund University, Faculty of Medicine.
2. *Faktablad Cancerstatistik, Sverige - Bröst*. 2019, NORDCAN, Association of the Nordic Cancer Registries.
3. Förnvik, H., *Optimization of breast tomosynthesis: Computer simulations of image acquisition and glandular dose.* 2018.
4. *Screening för bröstcancer - Rekommendationer och bedömningsunderlag*. 2014.
5. Carlson, P., *Mammografin utökas till alla över 40 år*, in *HELSINGBORGS DAGBLAD*. 2009.
6. *Breast cancer in Young Women*. 2017 [cited 2019 04 02]; Available from: https://www.webmd.com/breast-cancer/breast-cancer-young-women#1.
7. *Picture of the Breast - Human Anatomy*. 2005-2018 [cited 2018 11 09]; Available from: https://www.webmd.com/women/picture-of-the-breasts#1.
8. *The Pioneers of Mammography The difficult beginnings of a unique X-ray technology*. 2018 [cited 2018 11 13]; Available from: https://www.medmuseum.siemens.com/en/stories-from-the-museum/mammography.
9. Richard H. Gold, L.W.B., Bobbi E. Widoff, *Radiologic History Exhibit - Highlights from the History of Mammography.* RadioGraphics. **10**(6).
10. Shampo, M.A. and R.A. Kyle, *Pioneers of Mammography—Warren and Egan.* Mayo Clinic Proceedings, 1997. **72**(1): p. 32.
11. Björck, I., *Tomosyntes - nytt sätt att hitta bröstcancer*, in *Lunds Universitets Magasin, LUM*. 2015, Lunds Universitet.
12. Nyström, L., et al., *Reduced breast cancer mortality after 20+ years of follow-up in the Swedish randomized controlled mammography trials in Malmö, Stockholm, and Göteborg.* Journal of Medical Screening, 2017. **24**(1): p. 34-42.
13. Lång, K., *Breast tomosynthesis–new perspectives on breast cancer screening*. Vol. 2015. 2015: Lund University.
14. Zackrisson, S., et al., *One-view breast tomosynthesis versus two-view mammography in the Malmö Breast Tomosynthesis Screening Trial (MBTST): a prospective, population-based, diagnostic accuracy study.* The Lancet Oncology, 2018. **19**(11): p. 1493-1503.
15. van Schie, G., et al., *Generating synthetic mammograms from reconstructed tomosynthesis volumes.* IEEE transactions on medical imaging, 2013. **32**(12): p. 2322-2331.

16. Förnvik, D., et al., *The effect of reduced breast compression in breast tomosynthesis: human observer study using clinical cases.* Radiation Protection Dosimetry, 2010. **139**(1-3): p. 118-123.
17. Andersson, I., *Introduction to mammography*. 1992: A NICER Publication.
18. Dustler, M. 2019.
19. Fisher, R., et al. *Fourier Transform*. 2003 [cited 2018 03 28]; Available from: http://homepages.inf.ed.ac.uk/rbf/HIPR2/fourier.htm.
20. Chen, L., C.K. Abbey, and J.M. Boone, *Association between power law coefficients of the anatomical noise power spectrum and lesion detectability in breast imaging modalities.* Physics in Medicine & Biology, 2013. **58**(6): p. 1663.
21. Bochud, F.O., et al., *Importance of anatomical noise in mammography*. Medical Imaging 1997. Vol. 3036. 1997: SPIE. 7.
22. Sprawls, P., *The Physical Principles of Medical Imaging, 2nd Ed.* Sprawls Education Foundation.
23. Burgess, A.E., F.L. Jacobson, and P.F. Judy, *Human observer detection experiments with mammograms and power-law noise.* Medical physics, 2001. **28**(4): p. 419-437.
24. Burgess, A.E. and P.F. Judy, *Signal detection in power-law noise: effect of spectrum exponents.* JOSA A, 2007. **24**(12): p. B52-B60.
25. Dustler, M., *PhD*. 2019.
26. *Location of Spatial Frequencies*. 2018 [cited 2019 03-11]; Available from: http://mriquestions.com/locations-in-k-space.html.
27. Lee, C.I., L.E. Chen, and J.G. Elmore, *Risk-based breast cancer screening: implications of breast density.* Medical Clinics, 2017. **101**(4): p. 725-741.
28. Boyd, N.F., et al., *Mammographic density and the risk and detection of breast cancer.* New England Journal of Medicine, 2007. **356**(3): p. 227-236.
29. Sartor, H., *Mammographic Density in Relation to Breast Cancer: Tumor Characteristics, Mode of Detection, and Density Assessments*. 2015: Lund University.
30. *ACR BI-RADS ATLAS - MAMMOGRAPHY*. [cited 2019 02 13]; Available from: https://www.acr.org/-/media/ACR/Files/RADS/BI-RADS/Mammography-Reporting.pdf.
31. Kayar, R., et al., *Five methods of breast volume measurement: a comparative study of measurements of specimen volume in 30 mastectomy cases.* Breast cancer: basic and clinical research, 2011. **5**: p. BCBCR. S6128.
32. Ko, S.Y., et al., *Mammographic density estimation with automated volumetric breast density measurement.* Korean journal of radiology, 2014. **15**(3): p. 313-321.
33. van Engeland, S., et al., *Volumetric breast density estimation from full-field digital mammograms.* IEEE transactions on medical imaging, 2006. **25**(3): p. 273-282.

34. Keller, B.M., et al., *Preliminary evaluation of the publicly available Laboratory for Breast Radiodensity Assessment (LIBRA) software tool: comparison of fully automated area and volumetric density measures in a case–control study with digital mammography.* Breast Cancer Research, 2015. **17**(1): p. 117.
35. Conant, E.F., et al., *Agreement between breast percentage density estimations from standard-dose versus synthetic digital mammograms: Results from a large screening cohort using automated measures.* Radiology, 2017. **283**(3): p. 673-680.
36. Keller, B.M., et al., *Estimation of breast percent density in raw and processed full field digital mammography images via adaptive fuzzy c-means clustering and support vector machine segmentation.* Medical physics, 2012. **39**(8): p. 4903-4917.
37. Kooi, T., et al., *Large scale deep learning for computer aided detection of mammographic lesions.* Medical image analysis, 2017. **35**: p. 303-312.
38. Bahl, M., *Detecting Breast Cancers with Mammography: Will AI Succeed Where Traditional CAD Failed?* 2018, Radiological Society of North America.
39. Rodríguez-Ruiz, A., et al., *Detection of Breast Cancer with Mammography: Effect of an Artificial Intelligence Support System.* Radiology, 2018: p. 181371.
40. Rodriguez-Ruiz, A., et al., *Stand-alone artificial intelligence for breast cancer detection in mammography: comparison with 101 radiologists.* 2018.
41. Lång, K., et al., *Can artificial intelligence improve the balance of benefits and harms in breast cancer screeninng?* To be submitted, 2019.
42. Fredenberg, E. *Noise-Power Spectrum*. 2014 [cited 2018 10 18]; Available from: https://se.mathworks.com/matlabcentral/fileexchange/36462-noise-power-spectrum.
43. Engmann, N.J., et al., *Longitudinal changes in volumetric breast density with tamoxifen and aromatase inhibitors.* Cancer Epidemiology and Prevention Biomarkers, 2017. **26**(6): p. 930-937.

9 Appendices

9.1 Appendix 1

usecreateROI

```
a_segment = a > 0;   %tar fram allt som inte är svart dvs har
pixelvärde 0.
vector = find(a_segment); %en radvektor som motsvarar
elementvärdet som finns i a_segmentmatrisen. Varje element har
ett namn som är ett elementvärde.

mixIndex = randperm(length(vector)); %vektorn vector är
blandad, värdena som varje element har är ett övre vänstra
hörnet
mixVector = vector(mixIndex);
[m, n] = size(a);
s = [m, n];
vektorI = 1:100;          %skapa en vektor att spara hörnen i
vektorJ = 1:100;          %skapa en vektor att spara hörnen i
i = 0;
count = 1;
while count < 101
    i = i + 1;
    [I, J] = ind2sub(s,mixVector(i));

    while I+99 > m || J+99 > n            %denna ska köras om
om det högre hörnet hamnar utanför a-matrisen
        i = i + 1;                       %flyttar framåt i den
slumpade vektorn vector för platsen i som den var på gjorde
ett roi som var utanför bröstet.
        [I, J] = ind2sub(s,mixVector(i));
    end


    roi = a_segment(I:I+99, J:J+99);

    while sum(sum(roi)) ~= 10000         % ej lika med'
100*100 matris med 1:or summa=10000.
        i = i + 1;                       %flyttar framåt i den
slumpade vektorn vector för platsen i som den var på gjorde
ett roi som var utanför bröstet.
        [I, J] = ind2sub(s,mixVector(i));

        while I+99 > m || J+99 > n           %denna ska köras
om, om det högre hörnet hamnar utanför a-matrisen
            i = i + 1;                      %flyttar framåt i
den slumpade vektorn vector för platsen i som den var på
gjorde ett roi som var utanför bröstet.
            [I, J] = ind2sub(s,mixVector(i));
```

```
        end

        roi = a_segment(I:I+99, J:J+99);
    end

    vektorJ(count) = J;
    vektorI(count) = I;
    count = count + 1;
end

%Det är I och J som ska användas för att skapa ROIen på
bröstet, det som är
%testat nu är så att ROIerna innehåller 1 på alla platser.

%Detta ska nu göras om så att det plockas ut ur själva
bröstbilden.

a1 = a(vektorI(1):vektorI(1)+99, vektorJ(1):vektorJ(1)+99);
a2 = a(vektorI(2):vektorI(2)+99, vektorJ(2):vektorJ(2)+99);
a3 = a(vektorI(3):vektorI(3)+99, vektorJ(3):vektorJ(3)+99);
a4 = a(vektorI(4):vektorI(4)+99, vektorJ(4):vektorJ(4)+99);
a5 = a(vektorI(5):vektorI(5)+99, vektorJ(5):vektorJ(5)+99);
a6 = a(vektorI(6):vektorI(6)+99, vektorJ(6):vektorJ(6)+99);
a7 = a(vektorI(7):vektorI(7)+99, vektorJ(7):vektorJ(7)+99);
a8 = a(vektorI(8):vektorI(8)+99, vektorJ(8):vektorJ(8)+99);
a9 = a(vektorI(9):vektorI(9)+99, vektorJ(9):vektorJ(9)+99);
a10 = a(vektorI(10):vektorI(10)+99,
vektorJ(10):vektorJ(10)+99);

a11 = a(vektorI(11):vektorI(11)+99,
vektorJ(11):vektorJ(11)+99);
a12 = a(vektorI(12):vektorI(12)+99,
vektorJ(12):vektorJ(12)+99);
a13 = a(vektorI(13):vektorI(13)+99,
vektorJ(13):vektorJ(13)+99);
a14 = a(vektorI(14):vektorI(14)+99,
vektorJ(14):vektorJ(14)+99);
a15 = a(vektorI(15):vektorI(15)+99,
vektorJ(15):vektorJ(15)+99);
a16 = a(vektorI(16):vektorI(16)+99,
vektorJ(16):vektorJ(16)+99);
a17 = a(vektorI(17):vektorI(17)+99,
vektorJ(17):vektorJ(17)+99);
```

```
a18 = a(vektorI(18):vektorI(18)+99,
vektorJ(18):vektorJ(18)+99);
a19 = a(vektorI(19):vektorI(19)+99,
vektorJ(19):vektorJ(19)+99);
a20 = a(vektorI(20):vektorI(20)+99,
vektorJ(20):vektorJ(20)+99);

a21 = a(vektorI(21):vektorI(21)+99,
vektorJ(21):vektorJ(21)+99);
a22 = a(vektorI(22):vektorI(22)+99,
vektorJ(22):vektorJ(22)+99);
a23 = a(vektorI(23):vektorI(23)+99,
vektorJ(23):vektorJ(23)+99);
a24 = a(vektorI(24):vektorI(24)+99,
vektorJ(24):vektorJ(24)+99);
a25 = a(vektorI(25):vektorI(25)+99,
vektorJ(25):vektorJ(25)+99);
a26 = a(vektorI(26):vektorI(26)+99,
vektorJ(26):vektorJ(26)+99);
a27 = a(vektorI(27):vektorI(27)+99,
vektorJ(27):vektorJ(27)+99);
a28 = a(vektorI(28):vektorI(28)+99,
vektorJ(28):vektorJ(28)+99);
a29 = a(vektorI(29):vektorI(29)+99,
vektorJ(29):vektorJ(29)+99);
a30 = a(vektorI(30):vektorI(30)+99,
vektorJ(30):vektorJ(30)+99);

a31 = a(vektorI(31):vektorI(31)+99,
vektorJ(31):vektorJ(31)+99);
a32 = a(vektorI(32):vektorI(32)+99,
vektorJ(32):vektorJ(32)+99);
a33 = a(vektorI(33):vektorI(33)+99,
vektorJ(33):vektorJ(33)+99);
a34 = a(vektorI(34):vektorI(34)+99,
vektorJ(34):vektorJ(34)+99);
a35 = a(vektorI(35):vektorI(35)+99,
vektorJ(35):vektorJ(35)+99);
a36 = a(vektorI(36):vektorI(36)+99,
vektorJ(36):vektorJ(36)+99);
a37 = a(vektorI(37):vektorI(37)+99,
vektorJ(37):vektorJ(37)+99);
a38 = a(vektorI(38):vektorI(38)+99,
vektorJ(38):vektorJ(38)+99);
```

```
a39 = a(vektorI(39):vektorI(39)+99,
vektorJ(39):vektorJ(39)+99);
a40 = a(vektorI(40):vektorI(40)+99,
vektorJ(40):vektorJ(40)+99);

a41 = a(vektorI(41):vektorI(41)+99,
vektorJ(41):vektorJ(41)+99);
a42 = a(vektorI(42):vektorI(42)+99,
vektorJ(42):vektorJ(42)+99);
a43 = a(vektorI(43):vektorI(43)+99,
vektorJ(43):vektorJ(43)+99);
a44 = a(vektorI(44):vektorI(44)+99,
vektorJ(44):vektorJ(44)+99);
a45 = a(vektorI(45):vektorI(45)+99,
vektorJ(45):vektorJ(45)+99);
a46 = a(vektorI(46):vektorI(46)+99,
vektorJ(46):vektorJ(46)+99);
a47 = a(vektorI(47):vektorI(47)+99,
vektorJ(47):vektorJ(47)+99);
a48 = a(vektorI(48):vektorI(48)+99,
vektorJ(48):vektorJ(48)+99);
a49 = a(vektorI(49):vektorI(49)+99,
vektorJ(49):vektorJ(49)+99);
a50 = a(vektorI(50):vektorI(50)+99,
vektorJ(50):vektorJ(50)+99);

a51 = a(vektorI(51):vektorI(51)+99,
vektorJ(51):vektorJ(51)+99);
a52 = a(vektorI(52):vektorI(52)+99,
vektorJ(52):vektorJ(52)+99);
a53 = a(vektorI(53):vektorI(53)+99,
vektorJ(53):vektorJ(53)+99);
a54 = a(vektorI(54):vektorI(54)+99,
vektorJ(54):vektorJ(54)+99);
a55 = a(vektorI(55):vektorI(55)+99,
vektorJ(55):vektorJ(55)+99);
a56 = a(vektorI(56):vektorI(56)+99,
vektorJ(56):vektorJ(56)+99);
a57 = a(vektorI(57):vektorI(57)+99,
vektorJ(57):vektorJ(57)+99);
a58 = a(vektorI(58):vektorI(58)+99,
vektorJ(58):vektorJ(58)+99);
a59 = a(vektorI(59):vektorI(59)+99,
vektorJ(59):vektorJ(59)+99);
```

```
a60 = a(vektorI(60):vektorI(60)+99,
vektorJ(60):vektorJ(60)+99);

a61 = a(vektorI(61):vektorI(61)+99,
vektorJ(61):vektorJ(61)+99);
a62 = a(vektorI(62):vektorI(62)+99,
vektorJ(62):vektorJ(62)+99);
a63 = a(vektorI(63):vektorI(63)+99,
vektorJ(63):vektorJ(63)+99);
a64 = a(vektorI(64):vektorI(64)+99,
vektorJ(64):vektorJ(64)+99);
a65 = a(vektorI(65):vektorI(65)+99,
vektorJ(65):vektorJ(65)+99);
a66 = a(vektorI(66):vektorI(66)+99,
vektorJ(66):vektorJ(66)+99);
a67 = a(vektorI(67):vektorI(67)+99,
vektorJ(67):vektorJ(67)+99);
a68 = a(vektorI(68):vektorI(68)+99,
vektorJ(68):vektorJ(68)+99);
a69 = a(vektorI(69):vektorI(69)+99,
vektorJ(69):vektorJ(69)+99);
a70 = a(vektorI(70):vektorI(70)+99,
vektorJ(70):vektorJ(70)+99);

a71 = a(vektorI(71):vektorI(71)+99,
vektorJ(71):vektorJ(71)+99);
a72 = a(vektorI(72):vektorI(72)+99,
vektorJ(72):vektorJ(72)+99);
a73 = a(vektorI(73):vektorI(73)+99,
vektorJ(73):vektorJ(73)+99);
a74 = a(vektorI(74):vektorI(74)+99,
vektorJ(74):vektorJ(74)+99);
a75 = a(vektorI(75):vektorI(75)+99,
vektorJ(75):vektorJ(75)+99);
a76 = a(vektorI(76):vektorI(76)+99,
vektorJ(76):vektorJ(76)+99);
a77 = a(vektorI(77):vektorI(77)+99,
vektorJ(77):vektorJ(77)+99);
a78 = a(vektorI(78):vektorI(78)+99,
vektorJ(78):vektorJ(78)+99);
a79 = a(vektorI(79):vektorI(79)+99,
vektorJ(79):vektorJ(79)+99);
a80 = a(vektorI(80):vektorI(80)+99,
vektorJ(80):vektorJ(80)+99);
```

```
a81 = a(vektorI(81):vektorI(81)+99,
vektorJ(81):vektorJ(81)+99);
a82 = a(vektorI(82):vektorI(82)+99,
vektorJ(82):vektorJ(82)+99);
a83 = a(vektorI(83):vektorI(83)+99,
vektorJ(83):vektorJ(83)+99);
a84 = a(vektorI(84):vektorI(84)+99,
vektorJ(84):vektorJ(84)+99);
a85 = a(vektorI(85):vektorI(85)+99,
vektorJ(85):vektorJ(85)+99);
a86 = a(vektorI(86):vektorI(86)+99,
vektorJ(86):vektorJ(86)+99);
a87 = a(vektorI(87):vektorI(87)+99,
vektorJ(87):vektorJ(87)+99);
a88 = a(vektorI(88):vektorI(88)+99,
vektorJ(88):vektorJ(88)+99);
a89 = a(vektorI(89):vektorI(89)+99,
vektorJ(89):vektorJ(89)+99);
a90 = a(vektorI(90):vektorI(90)+99,
vektorJ(90):vektorJ(90)+99);

a91 = a(vektorI(91):vektorI(91)+99,
vektorJ(91):vektorJ(91)+99);
a92 = a(vektorI(92):vektorI(92)+99,
vektorJ(92):vektorJ(92)+99);
a93 = a(vektorI(93):vektorI(93)+99,
vektorJ(93):vektorJ(93)+99);
a94 = a(vektorI(94):vektorI(94)+99,
vektorJ(94):vektorJ(94)+99);
a95 = a(vektorI(95):vektorI(95)+99,
vektorJ(95):vektorJ(95)+99);
a96 = a(vektorI(96):vektorI(96)+99,
vektorJ(96):vektorJ(96)+99);
a97 = a(vektorI(97):vektorI(97)+99,
vektorJ(97):vektorJ(97)+99);
a98 = a(vektorI(98):vektorI(98)+99,
vektorJ(98):vektorJ(98)+99);
a99 = a(vektorI(99):vektorI(99)+99,
vektorJ(99):vektorJ(99)+99);
a100 = a(vektorI(100):vektorI(100)+99,
vektorJ(100):vektorJ(100)+99);
```

9.2 Appendix 2

The following script is based on Erik Fredenberg's (Royal Institute of Technology, KTH, Sweden) script `demo_nps_package.m` and can be found on https://se.mathworks.com/matlabcentral/fileexchange/36462-noise-power-spectrum (2019-03-04). The script is modified to be able to fit the images in the project.

useomskrivningavcalcNPSbeta

```
A = {a1; a2; a3; a4; a5; a6; a7; a8; a9; a10; a11; a12; a13;
a14; a15; a16; a17; a18; a19; a20;
    a21; a22; a23; a24; a25; a26; a27; a28; a29; a30; a31;
a32; a33; a34; a35; a36; a37; a38; a39; a40;
    a41; a42; a43; a44; a45; a46; a47; a48; a49; a50; a51;
a52; a53; a54; a55; a56; a57; a58; a59; a60;
    a61; a62; a63; a64; a65; a66; a67; a68; a69; a70; a71;
a72; a73; a74; a75; a76; a77; a78; a79; a80;
    a81; a82; a83; a84; a85; a86; a87; a88; a89; a90; a91;
a92; a93; a94; a95; a96; a97; a98; a99; a100;};
B = ones(length(A),1);

for i = 1:length(A)
    aaaa = A(i);
    aaaa = cell2mat(aaaa);

    I_3D = repmat(double(aaaa),[1 1 100]);


    %function [beta_vol,beta_proj,beta_slice] =
calcNPSbeta(I_3D)

    % Simulation of a 3D volume with power-law noise. Fractals
are examples of
    % structures that exhibit power-law NPS. These can be used
to describe many
    % naturally occuring phenomena such as mountains or
structures in the
    % human body. The latter includes, for instance, the
vascular system and
    % breast tissue, and the power-law noise may in that case
be used to model
    % the performance of a radiologist who interprets images
of the body.
    %
    % E. Fredenberg et al, RSNA 2011
    % E. Fredenberg et al, SPIE Medical Imaging 2011.
    % E. Fredenberg et al, Med Phys 37, 2017-2029 (2010).
    % Power-law NPS in 3D is very well described in:
    % Gang et al, Med Phys 37, 1948-1965 (2010).
```

```
    px = 85e-3;
    vx = 85e-3; % voxel side length [e.g. mm]
    n = 3; % number of dimensions

    % % Generate a 3D NPS.
    % % Magnitude of the power law.
    alpha = 1e-3;
    % % Exponent of the power law. beta = 0 is white noise,
beta = 1 is referred
    % % to as pink noise, beta = 2 is brown (or red) noise,
beta = 3 is
    % % sometimes called black noise. A space-filling fractal
has a
    % % characteristic power law with exponent beta = 3, and
many natural
    % % processes, for instance the vascular system or breast
tissue, have
    % % characteristic power laws with beta in the range 2-3.
    beta = 3;
    %
    % nps_fun_in = @(varargin) power_law_noise([alpha beta],
varargin{:});
    %
    % % Create a noise volume from the NPS.
    roi_size = 100; % The volume is 100x100x100 voxels
    % voxel_value = 0.5*vx; % This implies a volume that is,
for instance, half filled with a material.
    % stack_size = 1; % A single realization.
    % [I_3D, x] = filtered_noise(roi_size, n, stack_size,
voxel_value, vx, nps_fun_in);
    %
    % % Create a projection image from the volume.
    I_2D = sum(I_3D,3);

    % Measure the NPS
    use_window = 1; % Tapering window to avoid spectral
leakage.
    % in the 3D volume:
    average_rois = 0; % No averaging since there is only one
realization.
    [nps_3D_measured, f_x] = calc_digital_nps(I_3D, n, vx,
use_window, average_rois); % [e.g. mm^3]
    % in a slice of the 3D volume:
    average_rois = 1; % Use the planes as realizations.
    nps_slc_measured = calc_digital_nps(I_3D, n-1, vx,
use_window, average_rois);  % [e.g. mm^2]
    % in the projection:
    average_rois = 0;
    nps_2D_measured = calc_digital_nps(I_2D, n-1, vx,
use_window, average_rois); % [e.g. mm^2]
```

```
    % Assume rotational symmetry and convert to radial
coordinates.
    uniquify = 1;
    [nps_3Dr_measured, f_3Dr] = cart2rad(nps_3D_measured, f_x,
n, uniquify);
    [nps_slcr_measured, f_slcr] = cart2rad(nps_slc_measured,
f_x, n-1, uniquify);
    [nps_2Dr_measured, f_2Dr] = cart2rad(nps_2D_measured, f_x,
n-1, uniquify);

    % Fit the measured NPS:
    f_Nyq = 1/(2*px); % Nyquist frequency
    f_fit = logspace(log10(1/roi_size), log10(f_Nyq), 1000); %
log-spaced frequency vector
    log_fit = 1; % fit in log domain
    nps_fun_fit = @(P, varargin) power_law_noise(P,
varargin{:});
    % in the 3D volume:
    P_start_3D = [alpha beta];
    [P_fit_3D, nps_3Dr_fit] = fit_nps(nps_3Dr_measured, f_3Dr,
1, nps_fun_fit, P_start_3D, f_fit, log_fit);
    % in the slice:
    % slice alpha is found via the hypergeometric function,
slice beta is
    % volume beta-1. (Gang et al, Med Phys 37, 1948-1965
(2010))
    F = quadgk(@(p) (1+p.^2).^(-beta/2),0,Inf);
    P_start_slc = [2*alpha*F beta-1];
    [P_fit_slc, nps_slcr_fit] = fit_nps(nps_slcr_measured,
f_slcr, 1, nps_fun_fit, P_start_slc, f_fit, log_fit);
    % in the projection image
    P_start_2D = [alpha*roi_size/vx beta];
    [P_fit_2D, nps_2D_fit] = fit_nps(nps_2Dr_measured, f_slcr,
1, nps_fun_fit, P_start_2D, f_fit, log_fit);

    beta_vol =  num2str(P_fit_3D(2),2);

    beta_slice = num2str(P_fit_slc(2),2);

    beta_proj = num2str(P_fit_2D(2),2);

    beta_slice = str2double(beta_slice);

    B(i,1) = beta_slice;
end

%Körs då alla små delmatriser i A körts och då matrisen B är
fylld med beta_slice-värden.
```

```
summa = sum(B)
meanbeta = summa/(length(B))
```

9.3 Appendix 3

```
meanBetagammalsynthetic = zeros(1,409);
parfor numberImage = 1:409
    a = dicomread(gammalsyntfiler{numberImage});
    meanBetagammalsynthetic(numberImage) = idioticFunction(a);
end
```

9.4 Appendix 4

```
function out = idioticFunction(a)
usecreateROI
useomskrivningavcalcNPSbeta
out = meanbeta;
end
```

9.5 Appendix 5

The following four scripts (`calc_digital_nps(I, n, px, use_window, average_stack)`, `cart2rad(nps_x, f_x, n, unq)`, `fit_nps(nps_in, f_in, n, nps_fun, P_start, f_fit, log_fit)`, `power_law_noise(P, varargin)`) from https://se.mathworks.com/matlabcentral/fileexchange/36462-noise-power-spectrum (2019-03-04) by Erik Fredenberg were used in their original form.

9.5.1 calc_digital_nps(I, n, px, use_window, average_stack)

```
function [nps, f] = calc_digital_nps(I, n, px, use_window,
average_stack)
% [nps, f] = calc_digital_nps(I, n, px, use_window,
average_stack)
%
% Calculates the digital noise-power spectrum (NPS) noise-only
% realizations. The following rference provides a good
overview of NPS
% calculations:
% I. A. Cunningham, in Handbook of Medical Imaging (SPIE
Press,
% Bellingham, USA, 2000), vol. 1.
%
% I is a stack of symmetric n-dimensional noise realizations.
The
% realizations are stacked along the last array dimension of
I. If
% average_stack is set, the calculated NPS is averaged over
the stack to
% reduce uncertainty. px is the pixel size of the image.
%
% If use_window is set, the data is multiplied with a Hann
tapering window
% prior to NPS calculation. Windowing is useful for avoiding
spectral
% leakage in case the NPS increases rapidly towards lower
spatial
% frequencies (e.g. power-law behaviour).
%
% nps is the noise-power spectrum of I in units of px^n, and f
is the
% corresponding frequency vector.
%
% Erik Fredenberg, Royal Institute of Technology (KTH) (2010).
% Please reference this package if you find it useful.
% Feedback is welcome: fberg@kth.se.
if nargin<3 || isempty(px), px=1; end
if nargin<4 || isempty(use_window), use_window=0; end
```

```
if nargin<5 || isempty(average_stack), average_stack=0; end
stack_size=size(I,n+1);
size_I=size(I);
if any(diff(size_I(1:n)))
    error('ROI must be symmetric.');
end
roi_size=size_I(1);
% Cartesian coordinates
x=linspace(-roi_size/2,roi_size/2,roi_size);
x=repmat(x',[1 ones(1,n-1)*roi_size]);
% frequency vector
f=linspace(-0.5,0.5,roi_size)/px;
% radial coordinates
r2=0; for p=1:n, r2=r2+shiftdim(x.^2,p-1); end, r=sqrt(r2);
% Hann window to avoid spectral leakage
if use_window
    h=0.5*(1+cos(pi*r/(roi_size/2)));
    h(r>roi_size/2)=0;
    h=repmat(h,[ones(1,n) stack_size]);
else h=1;
end
% detrending by subtracting the mean of each ROI
% more advanced schemes include subtracting a surface, but
that is
% currently not included
S=I; for p=1:n, S=repmat(mean(S,p), ((1:n+1)==p)*(roi_size -
1) + 1); end
%S=repmat(S,ones(1,n)*roi_size);
F=(I-S).*h;
% equivalent to fftn
for p = 1:n, F = fftshift(fft(F,[],p),p); end
% cartesian NPS
nps=abs(F).^2/...
    roi_size^n*px^n./... NPS in units of px^n
    (sum(h(:).^2)/length(h(:))); % the normalization with h is
according to Gang 2010
% averaging the NPS over the ROIs assuming ergodicity
if average_stack, nps=mean(nps,n+1); end
```

9.5.2 cart2rad(nps_x, f_x, n, unq)

```
function [nps_r, f_r] = cart2rad(nps_x, f_x, n, unq)
% [nps_r, f_r] = cart2rad(nps_x, f_x, n, unq)
%
% Converts an n-dimensional symmetric noise-power spectrum
(NPS) from
% Cartesian to radial coordinates.
%
% Several NPS measurements may be stacked along the last array
```

```
% dimension of nps_x, which is indicated by ndim(nps_x) = n +
1. If unq is
% set, non-unique data points are averaged. This latter is a
slow function
% that should be improved.
%
% Erik Fredenberg, Royal Institute of Technology (KTH) (2010).
% Please reference this package if you find it useful.
% Feedback is welcome: fberg@kth.se.
% input checking
if nargin<4 || isempty(unq), unq=0; end
size_nps = size(nps_x); if any(diff(size_nps(1:n))),
error('ROI must be symmetric'); end
if length(size_nps)==2 && size_nps(1)==1, nps_x=nps_x'; end
roi_size = size(nps_x,1);
stack_size = size(nps_x,n+1);
% radial frequency vector
f_x=repmat(f_x',[1 ones(1,n-1)*roi_size]);
f_r2=0; for p=1:n, f_r2=f_r2+shiftdim(f_x.^2,p-1); end,
f_r=sqrt(f_r2);
% radial NPS
nps_r=reshape(nps_x,[roi_size^n stack_size]);
f_r=f_r(:);
% remove non-unique points if fitting in log domain because
% sum of log \neq log of sum
if unq, [f_r, nps_r]=uniquify(f_r, nps_r); end
end
function [A_out,B_out]=uniquify(A_in,B_in)
% Makes vectors unique for repetitive values in A_in by taking
the mean
% for the corresponding elements in B_in. This is a very slow
function that
% could be immensely improved.
if size(A_in,2)==1, A_in=A_in';
elseif size(A_in,1)~=1, error('A_in must be a vector')
end
if size(B_in,1)==size(A_in,2), B_in=B_in';
elseif size(B_in,1)==size(A_in,2), error('B_in must have one
dimension that matches A_in')
end
A_out=unique(A_in);
B_out=nan(size(B_in,1),size(A_out,2));
for a=1:numel(A_out)
    for b=1:size(B_in,1)
        B_out(b,a)=mean(B_in(b,A_in==A_out(a)));
    end
end
end
```

9.5.3 fit_nps(nps_in, f_in, n, nps_fun, P_start, f_fit, log_fit)

```
function [P_fit, nps_fit] = ...
    fit_nps(nps_in, f_in, n, nps_fun, P_start, f_fit, log_fit)
% [P_fit, nps_fit] = ...
%           fit_nps(nps_in, f_in, n, nps_fun, P_start, f_fit,
log_fit)
%
% Least-square fits a noise-power spectrum (NPS) to a
specified function
% and returns the parameters of the fit as well as the fitted
function.
%
% nps_fun is a handle to a function that accepts a parameter
vector P and n
% equally sized n-dimensional arrays with Cartesian
coordinates:
% nps_fun(P, f1, f2, ..., fn).
% Start values for the fit are supplied in P_start Frequency
vector for
% returning a fitted NPS are supplied in f_fit. Setting
log_fit returns a
% fit in the log domain, which is useful for large ranges of
data, such as
% for a power-law NPS.
%
% Erik Fredenberg, Royal Institute of Technology (KTH) (2010).
% Please reference this package if you find it useful.
% Feedback is welcome: fberg@kth.se.
% input checking
if nargin<4, f_fit = f_in; end
if nargin<5 || isempty(log_fit), log_fit=0; end
size_nps=size(nps_in);
if any(diff(size_nps(1:n)))
    error('ROI must be symmetric.');
end
if length(size_nps)==2 && size_nps(1)==1, nps_in=nps_in'; end
if size(f_in,1)==1, f_in=f_in'; end
roi_size = size(nps_in,1);
stack_size = size(nps_in,n+1); stack_size = max(stack_size,
1);
% frequency vectors
f_in_a = repmat(f_in, [1 ones(1, n-1)*roi_size]);
f_in_c = cell(1,n); for p = 1:n, f_in_c{p} = shiftdim(f_in_a,
p-1); end % create arrays similar to meshgrid
f_fit_a = repmat(f_fit', [1 ones(1, n-1)*roi_size]);
f_fit_c = cell(1,n); for p = 1:n, f_fit_c{p} =
shiftdim(f_fit_a, p-1); end  % create arrays similar to
meshgrid
fitting_options =
optimset('Display','off','FunValCheck','on');
```

```
P_fit=zeros(stack_size, length(P_start));
nps_fit=zeros(stack_size, length(f_fit));
for k=1:stack_size;

    nps_k = permute(nps_in, [n+1 1:n]);
    nps_k = ipermute(nps_k(k,:), [n+1 1:n]);
    if ~log_fit % lin fitting
        fit_fun = @(P) sum((nps_fun(P,f_in_c{:}) - nps_k).^2);
    elseif log_fit % log fitting
        fit_fun = @(P) sum((real(log(nps_fun(P,f_in_c{:}))) -
log(nps_k)).^2);
    end

    P_fit(k,:) = fminsearch(fit_fun, P_start,
fitting_options);

    nps_fit(k,:) = nps_fun(P_fit(k,:),f_fit_c{:});

end
end
```

9.5.4 power_law_noise(P, varargin)

```
function nps = power_law_noise(P, varargin)
% nps = power_law_noise(P(alpha, beta), f1, f2, ..., fn)
% nps = power_law_noise(P(alpha, beta), fr)
%
% Returns a radially symmetric power-law NPS, nps = alpha *
fr^(-beta), for
% Cartesian or radial input coordinates.
%
% f1, f2, ..., fn are equally sized n-dimensional arrays with
Cartesian
% coordinates. Optionally, fr is an array of radial
coordinates. The output
% nps is in Cartesian coordinates and in units of alpha.
%
% Erik Fredenberg, Royal Institute of Technology (KTH) (2010).
% Please reference this package if you find it useful.
% Feedback is welcome: fberg@kth.se.
% input checking
if length(varargin)>1 && (ndims(varargin{1})~=length(varargin)
||...
        any(diff(cellfun(@(C) ndims(C),varargin))))
    error('f1, f2, ..., fn need to be equally sized n-D
arrays.')
end
alpha = P(1);
```

```
beta = P(2);
% converting to radial coordinates
r2=0; for p = 1:length(varargin), r2 = r2 + varargin{p}.^2;
end
% power law
nps = alpha * r2.^(-beta/2);
```

9.6 Appendix 6

```
for i = 1:168
    image = dicomread(namn{i});
    info = dicominfo(namn{i});
    remove = rmfield (info, 'ImagesInAcquisition');
    a = ['H:\Ellinor fall för analys\' num2str(i) '.dcm'];
    dicomwrite(image,a,remove,'CreateMode','copy');
    filePaths{i} = a;
end
```

9.7 Appendix 7

```
for i = 1:length(namn);
    image = dicomread(namn{i});
    info = dicominfo(namn{i});
    type = info.ImageLaterality;          %denna tar fram
ImageType som ska ändras till 'DERIVED\PRIMARY\LEFT ELLER
RIGHT BEROENDE PÅ'
    if isequal(type,'R')    %jag tror att alla har denna typ av
ImageType, även vänster bröst.
        info.ImageType = 'DERIVED\PRIMARY\TOMO_2D\RIGHT';
        info.SeriesDescription = 'T_PR R-MLO PRIME,
Diagnosis';
    else
        info.ImageType = 'DERIVED\PRIMARY\TOMO_2D\LEFT';
        info.SeriesDescription = 'T_PR L-MLO PRIME,
Diagnosis';
    end

    info.ImagesInAcquisition = 1;
    info.AcquisitionNumber = 1;


    a = ['H:\Insight2D_raw\syntetiskachangedtags\' num2str(i)
'.dcm'];
    dicomwrite(image, a, info, 'CreateMode', 'Copy')
end
```

9.8 Appendix 8 – Results

The data received were all plotted in histograms to investigate the distribution of the data. Based on the data distribution, appropriate statistical analysis methods were chosen to investigate the data.

9.8.1 β – value

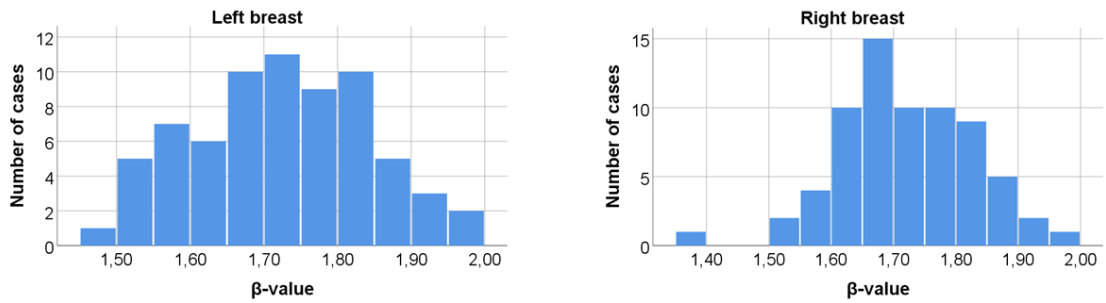

Figure 9.1: Distribution of the β-values for conventional mammograms.

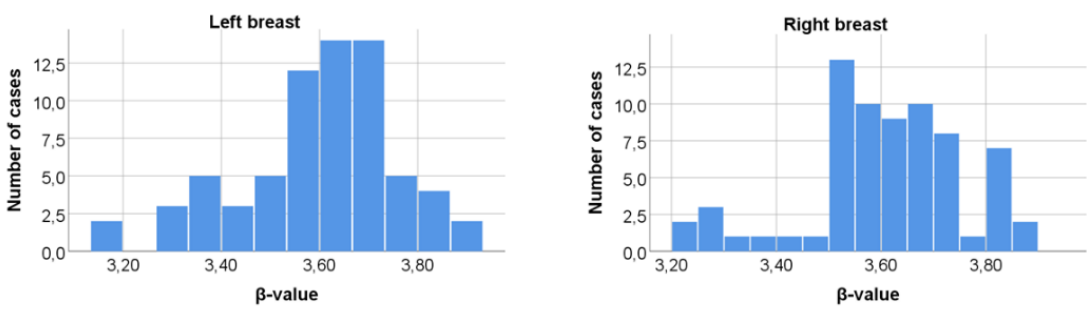

Figure 9.2: Distribution of the β-values for old Insight2D.

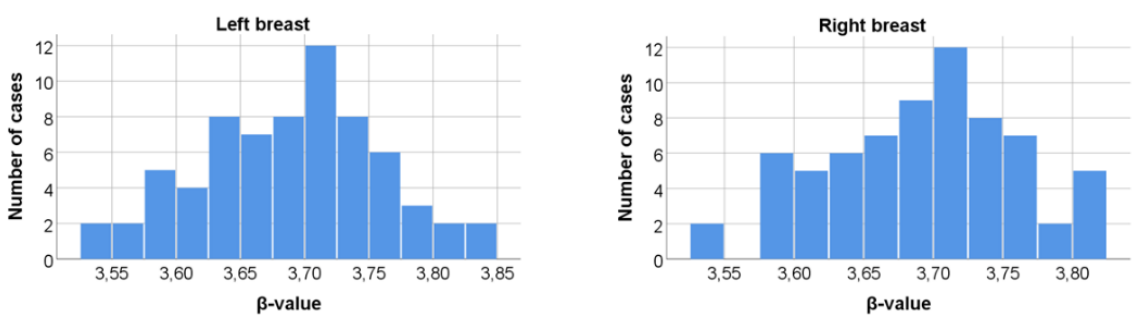

Figure 9.3: Distribution of the β-values for new Insight 2D.

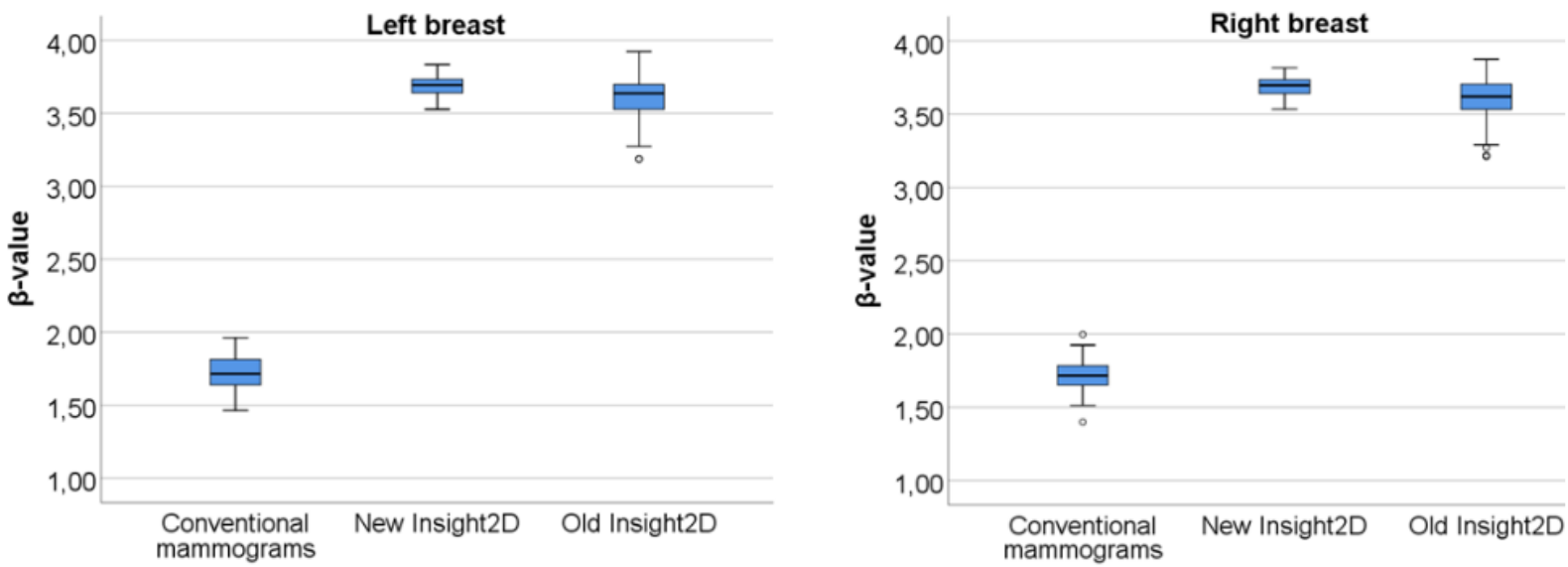

Figure 9.4: Boxplots for the β-values for the different kinds of mammograms showing left and right breast, respectively.

9.8.2 Density measurements

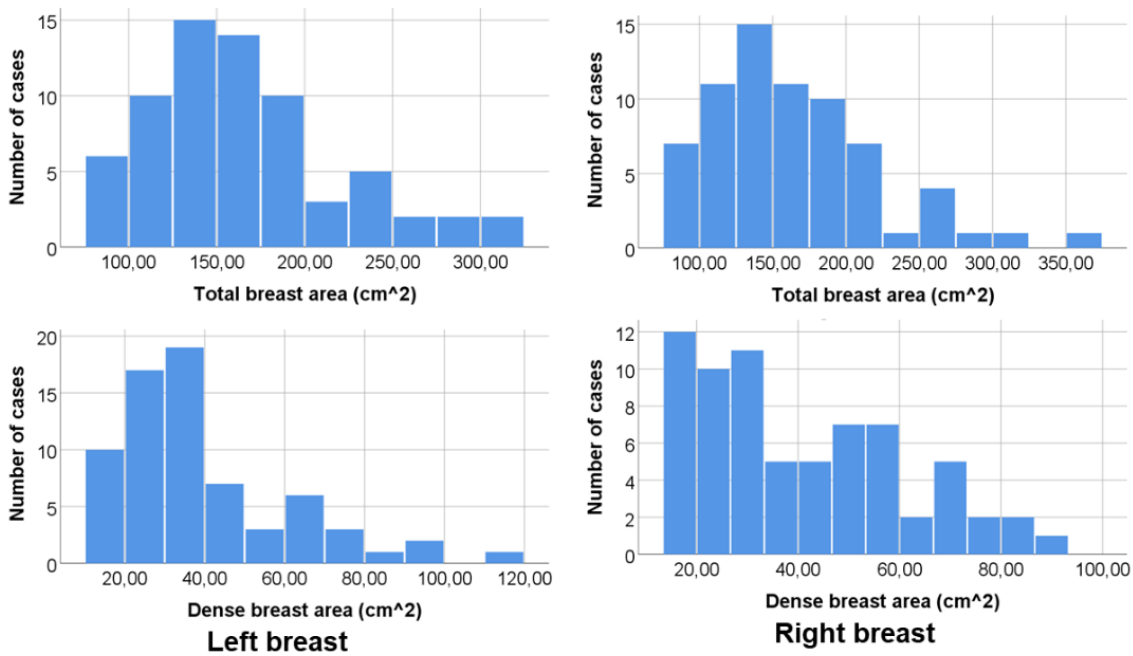

Figure 9.5: Total breast area and dense breast area for conventional mammograms.

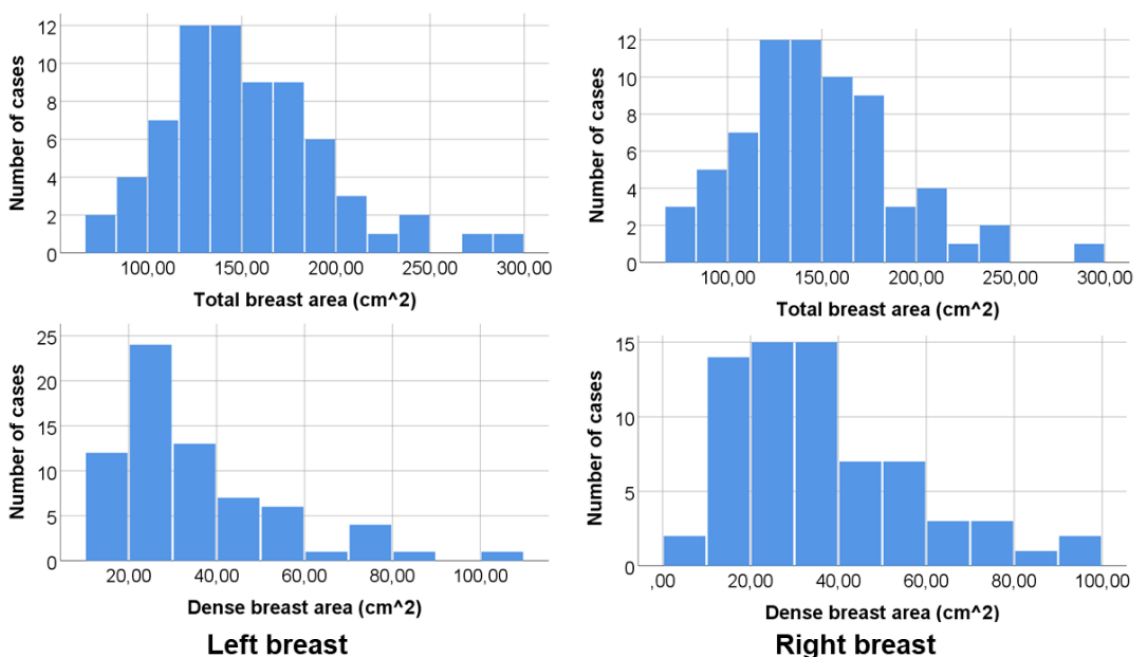

Figure 9.6: Total breast area and dense breast area for new Insight2D.

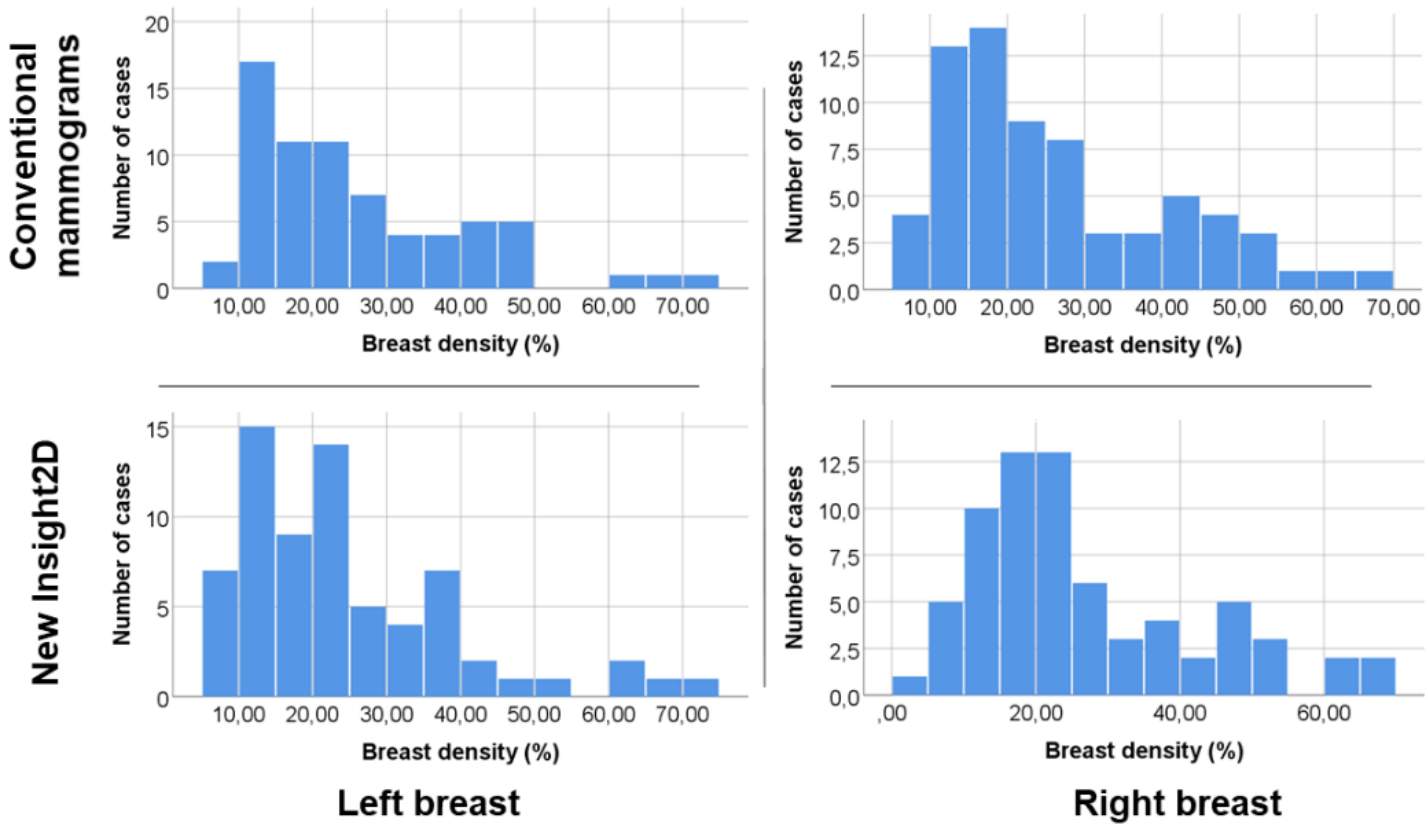

Figure 9.7: Breast density for conventional mammograms and new Insight2D, respectively.

9.8.3 Transpara score

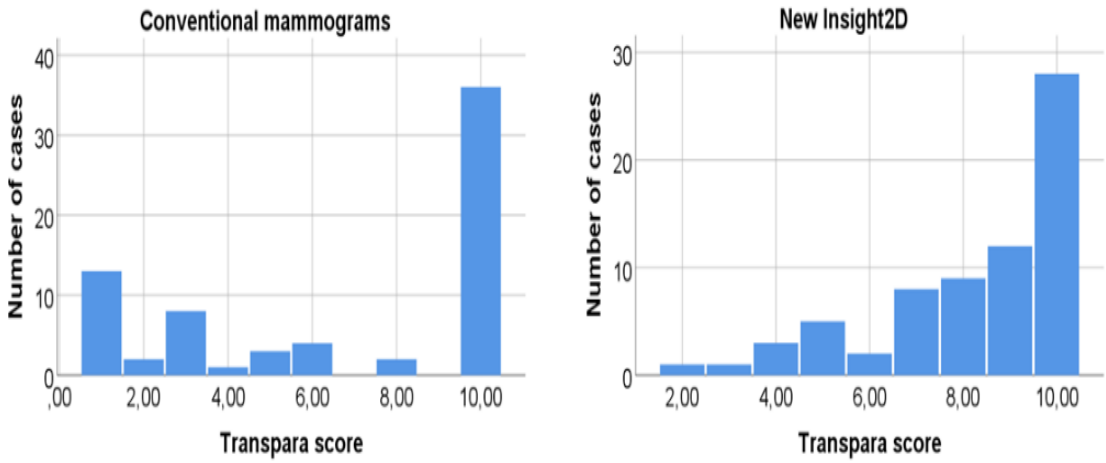

Figure 9.8: Transpara score distribution for conventional mammograms and new Insight2D, respectively.

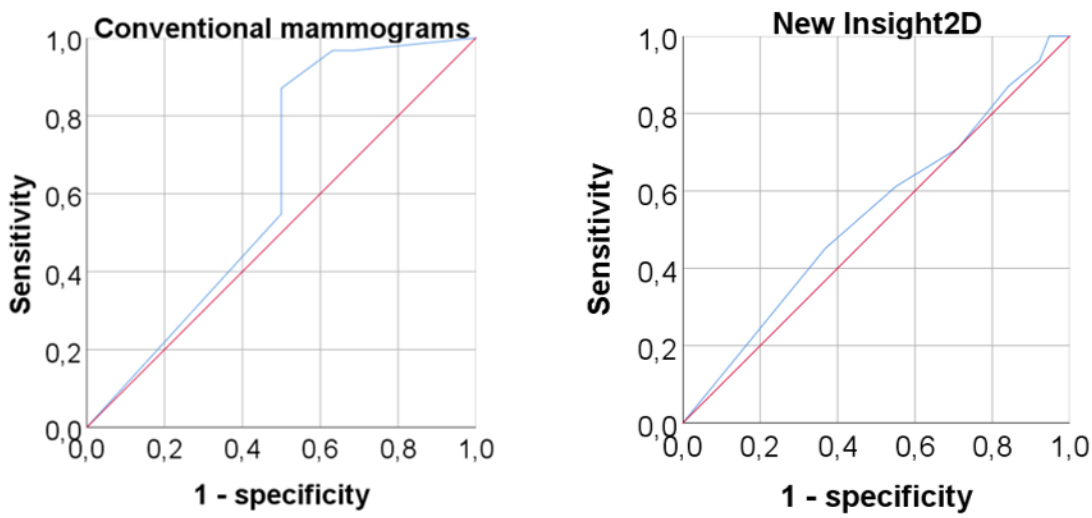

Figure 9.9: ROC curves for Transpara scores for conventional mammograms and new Insight2D, respectively.